Calmodulin binds to *Drosophila* TRP with an unexpected mode

Weidi Chen[1,2,7], Zeyu Shen[3,7], Sabrina Asteriti[4,6], Zijing Chen[5], Fei Ye[3], Ziling Sun[1], Jun Wan[1,2,3], Craig Montell[5], Roger C Hardie[4], Wei Liu[1,*], and Mingjie Zhang[1,2,3,8,*]

[1]Shenzhen Key Laboratory for Neuronal Structural Biology, Biomedical Research Institute, Shenzhen Peking University-The Hong Kong University of Science and Technology Medical Center, Shenzhen 518036, China

[2]Greater Bay Biomedical Innocenter, Shenzhen Bay Laboratory, Shenzhen 518055, China

[3]Division of Life Science, State Key Laboratory of Molecular Neuroscience, Hong Kong University of Science and Technology, Clear Water Bay, Kowloon, Hong Kong, China.

[4]Department of Physiology, Development and Neuroscience, Cambridge University, Downing St, Cambridge CB2 3EG, United Kingdom

[5]Department of Molecular, Cellular and Developmental Biology, and the Neuroscience Research Institute, University of California, Santa Barbara, Santa Barbara, CA 93106, United States

[6]Department of Neurosciences, Biomedicine and Movement Science, University of Verona, Verona, Italy

Running title: An unexpected binding mode between CaM and TRP

[7]These authors contributed equally to this work.

[8]Lead Contact

*Corresponding authors: Wei Liu (liuwei@sphmc.org) and Mingjie Zhang (mzhang@ust.hk)

Abstract

Drosophila TRP is a calcium-permeable cation channel essential for fly visual signal transduction. During phototransduction, Ca^{2+} mediates both positive and negative feedback regulation on TRP channel activity, possibly via binding to calmodulin (CaM). However, the molecular mechanism underlying Ca^{2+} modulated CaM/TRP interaction is poorly understood. Here, we discover an unexpected, Ca^{2+}-dependent binding mode between CaM and TRP. The TRP tail contains two CaM binding sites (CBS1 and CBS2) separated by a ~70-residue linker. CBS1 binds to the CaM N-lobe and CBS2 recognizes the CaM C-lobe, so each TRP only binds to one CaM. Mutations introduced in both CBS1 and CBS2 completely eliminated CaM binding in full length TRP, but surprisingly had no effect on the response to light under physiological conditions, suggesting alternative mechanisms governing Ca^{2+}-mediated feedback on the channel activity. Finally, we discover that TRPC4, the closest mammalian paralog of *Drosophila* TRP, adopts a similar CaM binding mode.

INTRODUCTION

Transient receptor potential channels (TRP channels) are extensively expressed in different species of animals and involved in diverse physiological processes such as responding to light, pressure, pain, taste, temperature, and other stimuli (Clapham, 2003; Montell, 2005). Based on their sequence similarities and functional properties, TRP channels in mammals can be classified into 7 subfamilies: the canonical TRP channels (TRPCs), the melastatin TRP channels (TRPMs), the vanilloid TRP channels (TRPVs), the polycystin channels (TRPPs), the ankyrin transmembrane protein 1 channels (TRPA), the mucolipin channels (TRPML) and mechanosensing TRPN channels (*Drosophila* NOMPC) (Li, 2017; Montell, 2005).

The archetype TRP channel was discovered ~30 years ago following investigations of a spontaneous *Drosophila* mutant which had abnormal electroretinogram during prolonged intense light stimulation (Cosens and Manning, 1969). The *Drosophila* TRP (referred to as TRP from hereon) protein was later shown to be a Ca^{2+} permeable cation channel essential for excitation and light adaptation in *Drosophila* phototransduction (Hardie and Minke, 1992; Minke and Selinger, 1996; Montell and Rubin, 1989; Suss-Toby et al., 1991). Underneath the plasma membranes of rhabdomere in *Drosophila* photoreceptor cells, TRP together with eye-specific protein kinase C (ePKC) and phospholipase Cβ (NORPA) are assembled by a master scaffold protein called inactivation no after potential D (INAD) into a large and stoichiometric supra-molecular assembly termed the signalplex or transducisome (Chevesich et al., 1997; Hardie and Raghu, 2001; Montell, 2012; Tsunoda et al., 1997; Ye et al., 2018; Ye et al., 2016).

As well as being a Ca^{2+}-permeable channel, the *Drosophila* TRP is also known to be regulated by Ca^{2+} ions (Hardie, 1991, 1995; Scott et al., 1997) and Ca^{2+} influx via the channels can exert both positive and negative feedback regulation on TRP activities. In the presence of physiological Ca^{2+}concentration, TRP can be activated and terminated with extremely fast kinetics (Hardie, 1991, 1995; Reuss et al., 1997).

Ca^{2+} influx also mediates light adaptation (Gu et al, 2005) and is critical for dark noise threshold maintenance in *Drosophila* photoreceptors (Chu et al., 2013; Katz and Minke, 2012). However, the molecular mechanisms by which Ca^{2+} regulates TRP activities are largely unknown. At least two potential non-exclusive mechanisms exist. First, Ca^{2+} may directly bind to TRP to regulate channel activities, as in the case recently demonstrated for mammalian TRPMs (Wang et al., 2018; Yin et al., 2019). Second, Ca^{2+} might indirectly regulate channel activity by modulating the interaction between TRP and calmodulin (CaM) (Chevesich et al., 1997; Sun et al., 2018; Tang et al., 2001). CaM, as a principal Ca^{2+} signal decoder in all eukaryotic cells, is known to bind to and regulate activities of various ion channels including voltage-gated K^+ channels (Chang et al., 2018), Na^+ channels (Herzog et al., 2003), Ca^{2+} channels (Qin et al., 1999), etc. For the TRP superfamily ion channels, CaM also serves as a channel regulator with versatile functions (Zhu, 2005). For example, CaM is critical for Ca^{2+}-mediated termination of TRPV5 and TRPV6 activity (Hughes et al., 2018; Singh et al., 2018). On the contrary, CaM seems to act as an activator of TRPC4 and TRPC5 (Ordaz et al., 2005; Otsuguro et al., 2008). In *Drosophila* compound eyes, reduction of CaM can markedly impair the termination process of phototransduction (Liu et al., 2008; Porter et al., 1995; Scott et al., 1997). CaM was demonstrated to directly bind to a large fragment of the TRP tail (aa L683-A976) using a CaM-overlay assay (Chevesich et al., 1997). However, the mechanisms for CaM to regulate TRP is poorly understood. Currently, there is no structural study on the binding of CaM to TRP.

In this study, we characterized the interaction between CaM and the C-terminal tail of TRP in detail. We demonstrated that the TRP tail contains two CaM binding sites (CBSs) separated by a flexible linker with more than 70 amino acid residues. Unexpectedly, we found that the TRP tail containing both CBSs binds to one molecule of Ca^{2+}-CaM with its CBS1 engaging the CaM N-lobe and CBS2 binding to the CaM C-lobe. Lys75 in the N-lobe of CaM plays a critical role in determining the specificity of the two CBS sites for binding to N- and C-lobes of CaM. Guided by the

biochemical binding mechanism and the structure of the TRP/CaM complex uncovered in this study, we searched for potential binding between CaM and mammalian TRPCs, and found that the mouse TRPC4 C-terminal tail binds to Ca^{2+}-CaM in a mode similar to that between CaM and *Drosophila* TRP. Together, our discoveries serve as a structural framework for future investigations of TRP channel activity regulation by Ca^{2+} and CaM.

RESULTS

Characterization of the interaction between *Drosophila* TRP C-terminal tail and CaM

We began our study by performing a detailed biochemical characterization of the interaction between CaM and the TRP tail. The tail of TRP begins with residue S717 and ends at residue L1275 (Figure 1A). Searching the Calmodulin Target Database (http://calcium.uhnres.utoronto.ca/ctdb/no_flash.html) (Yap et al., 2000) showed that the N-terminal part of the TRP tail (aa 717-940) contains several potential CaM binding sites, and the rest of the tail (aa 940-1275) does not contain signs of CaM binding sequence. Consistently, the C-terminal part of the tail (aa 940-1275, purified as a thioredoxin (Trx)-tagged fusion protein, had no detectable binding to CaM either in the presence or absence of Ca^{2+} (Figure 1B). In contrast, the N-terminal part of the TRP tail (aa 717-940) specifically bound to Ca^{2+}-CaM based on analytical gel filtration chromatography coupled with static light scattering (SLS). Using both Trx-tagged and tag-removed proteins, we calculated that TRP (aa 717-940) bound to Ca^{2+}-CaM with a 1:2 stoichiometry (Figure 1C), indicating that there are at least two CaM binding sites within the fragment.

We further divided the 717-940 fragment into two. Interestingly, the fragment containing aa 783-940 (we chose to start the fragment from N783 as this residue marks the beginning of non-conserved regions among the TRP channels following the

coiled-coil domain; Figure 1F) was found to bind to CaM in a Ca^{2+}-dependent manner, and this fragment (referred to as CBS-B in Figure 1A) binds to Ca^{2+}-CaM with a 1:1 stoichiometry (Figure 1D). The TRP fragment containing 717-783 could not be expressed in soluble forms alone or in complex with CaM in bacterial cells. We therefore used a synthetic peptide to test whether a certain segment in this region may bind to CaM. As was shown in an earlier study, a synthetic peptide corresponding aa 728-754 of TRP bound to Ca^{2+}-CaM with a Kd of 3.75±0.62 μM (Tang et al., 2001) (Figure 1E), and we refer this CaM binding site of TRP as CBS-A (Figure 1A). The residues corresponding to CBS-A largely overlap with the entire connecting helix in the closed state structures of TRPC3, TRPC4, TRPC5 and TRPC6 (Duan et al., 2018; Duan et al., 2019; Tang et al., 2018) (Figure 1F). The residues corresponding to aa 728-754 of TRP are predicted to form a single connecting helix that is completely buried in the structures of TRPCs (Figure 1G). Therefore, it is unlikely that the fragment corresponding to the CBS-A site of TRP is accessible to CaM in the closed state full-length channel. Thus, the interaction between CBS-A peptide and CaM may originate from an artifact of the TRP tail fragmentation from the intact channel. Indeed, we demonstrated that the CBS-A site in the full-length endogenous TRP is not involved in binding to CaM (see data in Figure 4 below). However, we cannot exclude the possibility that CBS-A may function as a CaM binding site of TRP under certain conditions when this part of TRP gets exposed. The above biochemical study, together with structure-based sequence analysis of TRP and TRPC channels, establishes that the TRP tail fragment encompassing residues 783-940 contains the functional CaM binding element.

The TRP tail contains two discrete CaM binding sites acting together to bind one CaM in a Ca^{2+}-dependent manner

Detailed sequence analysis of the 783-940 fragment of the TRP tail revealed two potential CaM binding sites (CBSs) with sequences conserved in insects, though not

in mammalian TRPCs (Figure 2A). These two potential CBS sequences are defined as CBS1 (aa T802-K862) and CBS2 (aa M899-D940), which we used for the following experiments, unless specified otherwise. We used purified Trx-fused CBS1 and CBS2 to test whether the predicted CBS fragments may indeed bind to CaM. Isothermal titration calorimetry (ITC)-based assays showed that CBS1 binds to Ca^{2+}-CaM with a K_d of 0.35±0.09 μM, and with a 1:1 stoichiometry (Figure 2B1). CBS2 also binds to Ca^{2+}-CaM with a 1:1 stoichiometry and a K_d of 0.25±0.03 μM (Figure 2B2). Neither CBS1 nor CBS2 showed detectable binding to apo-CaM (titration curves in red in Figure 2B). The data in Figure 2B reveal that both CBS1 and CBS2 can bind to CaM in a Ca^{2+}-dependent manner and with quite strong binding affinities. Unexpectedly, the analytical gel filtration chromatography coupled with static light scattering (SLS) analysis (Figure 1D), and analytical ultracentrifugation (AUC) sedimentation velocity analysis (Figure 2C) showed that a large fragment of TRP tail encompassing both CBS1 and CBS2 (aa N783-D940) formed a stable complex with Ca^{2+}-CaM with a 1:1 stoichiometry. In fact, the TRP(783-940)/Ca^{2+}-CaM complex could only be obtained by co-expressing the two proteins together in bacteria cells. Removal of Ca^{2+} from the complex by addition of an excess amount of EDTA led to dissociation of TRP(783-940) from CaM. Moreover, the dissociated TRP(783-940) precipitated due to its extremely low solubility (data not shown).

There are two possible explanations for the above observations. CBS1 and CBS2 may compete with each other for binding to CaM, so only one of the two CBS sites engages CaM in the TRP(783-940)/Ca^{2+}-CaM complex. Alternatively, CBS1 and CBS2 may simultaneously interact with one molecule of CaM, thus forming the 1:1 TRP(783-940)/Ca^{2+}-CaM complex. To differentiate between these two possibilities, we mixed CBS1, CBS2 and CaM at a 1:1:1 molar ratio and subjected the mixture to analytical gel-filtration coupled with SLS analysis. The CBS1/CBS2/CaM mixture eluted as a single peak with a volume smaller than the elution volume of the CBS1/CaM complex or the CBS2/CaM complex (Figure 2D, top). SDS-PAGE

analysis of the fractions of the elution peak of the CBS1/CBS2/CaM mixture also showed that CaM formed a complex simultaneously with Trx-CBS1 and Trx-CBS2 (Figure 2D, bottom). Taken together, the above analysis suggested that a stable triple complex was formed when CBS1, CBS2 and CaM were mixed at a 1:1:1 molar ratio (i.e. both CBS1 and CBS2 bind to the same Ca^{2+}-CaM moiety).

To further understand the molecular mechanism governing the interaction between CBS12 and CaM, we resorted to NMR spectroscopic studies. We compared the ^{1}H-^{15}N HSQC spectrum of Ca^{2+}-CaM co-expressed with CBS12 complex with the spectrum of Ca^{2+}-CaM and found that residues from both the N- and C-lobes of Ca^{2+}-CaM underwent significant CBS12 binding-induced chemical shift changes (Figure 2E, and Figure S1A&B for the whole spectra). These data indicate that both lobes of CaM are involved in the interaction with CBS12. To further dissect the interaction, we overlaid the ^{1}H-^{15}N HSQC spectrum of the ^{15}N-Ca^{2+}-CaM/CBS12 complex with that of the ^{15}N-Ca^{2+}-CaM/^{14}N-CBS1 complex or with that of the ^{15}N-Ca^{2+}-CaM/^{14}N-CBS2 complex. The ^{1}H-^{15}N HSQC spectrum of the Ca^{2+}-CaM in Ca^{2+}-CaM/CBS12 complex roughly overlapped with the summed spectra of ^{15}N-Ca^{2+}-CaM/^{14}N-CBS1 and ^{15}N-Ca^{2+}-CaM/^{14}N-CBS2 (Figure 2E and Figure S1B), suggesting that CBS1 and CBS2 bind to distinct lobes of Ca^{2+}-CaM. We also compared the ^{1}H-^{15}N HSQC spectrum of ^{15}N-labelled Ca^{2+}-CaM with that of ^{15}N-labelled Ca^{2+}-CaM in complex with unlabeled CBS1 or CBS2 (Figure S1A). The binding of CBS1 induced large chemical shift changes to the N-lobe of Ca^{2+}-CaM, but only caused relatively small shift changes to the C-lobe of CaM. Conversely, binding of CBS2 induced large chemical shift changes to the C-lobe of Ca^{2+}-CaM, but chemical shift changes to the N-lobe of CaM was small (see the signature Gly residues from each EF-hand of Ca^{2+}-CaM in the zoomed in region in Figure S1A). The above NMR analysis suggested that CBS1 and CBS2 specifically bind to the N-lobe and C-lobe of Ca^{2+}-CaM, respectively, such that Ca^{2+}-CaM and CBS12 form a stable 1:1 complex. To confirm the conclusion derived from the NMR-based study,

we generated CaM derivatives in which we mutated Ca^{2+}-binding sites in the N-lobe or the C-lobe by substituting the last Glu in EF-hands 1&2 with Gln (i.e. E31/67Q) or EF-hands 3&4 with Gln (i.e. E104/140Q). The E31/67Q-CaM lost its binding to CBS1 but retained its binding to CBS2. Conversely, the E104/140Q-CaM lost its CBS2 binding but retained CBS1 binding (Figure S2). Taken together, we formulate an interaction model between TRP(783-940) and Ca^{2+}-CaM (Figure 2F). In this model, CBS1 and CBS2 selectively bind to the N-lobe and C-lobe of Ca^{2+}-CaM, respectively, forming a stable 1:1 complex. It is noteworthy that the complete CaM binding region of the TRP tail spans a total of ~140 amino acid residues (Figure 2A).

Finally, we asked whether CBS12 might be able to bind to Ca^{2+}-CaM with a higher affinity due to potential synergistic actions of CBS1 and CBS2. Since we could not obtain isolated CBS12 for ITC-based assay, we used analytical ultracentrifugation (AUC) sedimentation equilibrium to measure the dissociation constant between CBS12 and CaM (Figure 2G). The K_d value (0.10±0.01 μM) derived from AUC for the Ca^{2+}-CaM/CBS12 complex is comparable to that of the Ca^{2+}-CaM/CBS1complex or the Ca^{2+}-CaM/CBS2 complex (Figure 2B), indicating that there is very little conformational coupling (or synergism) between CBS1 and CBS2 in binding to CaM.

Structural Characterization of the CaM/TRP CBS12 Complex

We attempted to uncover the detailed molecular mechanism governing the unexpected binding between TRP tail and CaM by determining the crystal structure of the CBS12/Ca^{2+}-CaM complex. Despite extensive trials, we could not crystallize the complex, likely due to the conformational flexibility between the two lobes of CBS12-bound Ca^{2+}-CaM (Figure 2F and the NMR data in Figure 2E and Figure S1). Since CBS1 and CBS2 independently bind to the N- and C-lobes of Ca^{2+}-CaM, we decided to crystallize the CBS1/N-lobe_CaM and CBS2/C-lobe_CaM complexes separately. We were able to determine the structures of CBS1/N-lobe_CaM complex

and CBS2/C-lobe_CaM complex at resolutions of 1.78Å and 2.15Å, respectively (Figure 3A and Figure S3 and Table 1). For easy viewing, we connected the two lobes of CaM by a dotted line representing the flexible central linker connecting αD and αE of Ca^{2+}-CaM.

Both lobes of CaM adopt an open conformation with a Ca^{2+} ion occupying each EF-hand (Zhang et al., 1995). Interestingly, CBS1 forms a "helix-turn-helix" structure interacting with the hydrophobic surface of N_lobe_CaM. The first helix (α1) spans Q816-M827 and the second helix (α2) encompasses I836-G845. The residues connecting the α1 and α2 are not defined in the structure. Both helices are amphipathic in nature (Figure 2A). The hydrophobic residues from α2 make extensive contacts with CaM and the side chain of F837 from α2 functions as the anchoring residue inserting into the deep pocket of N-lobe_CaM (Figure 3B). The hydrophobic residues from α1 of CBS1 also interact with CaM and with α2. The formation of a helix-turn-helix conformation of CBS1 while binding to one lobe of Ca^{2+}-CaM is rather unusual among the numerous CaM/target complexes determined to date (Hoeflich and Ikura, 2002; Tidow and Nissen, 2013). This also explains why an elongated fragment (>30 amino acid residues) is required for CBS1 to bind to the N-lobe_CaM. It is worth noting that the binding mode between the C-lobe of Ca^{2+}-CaM to a variant of the SK2 K^+-channel tail resembles the CBS1/N-lobe_CaM structure in this study, because the SK2 peptide also forms a helix-turn-helix conformation (Zhang et al., 2012). However, the first helix (corresponding to α1 in CBS1) in the SK2 channel does not make direct contact with CaM, whereas α1 in CBS1 interacts with CaM directly (Figure 3B).

CBS2 in the complex with the C-lobe_CaM forms a single α-helix (α3) spanning A917-K929 (Figure 2A and Figure 3C). Like most of other Ca^{2+}-CaM binding helical peptides (Tidow and Nissen, 2013), CBS2 α3 is also a positively charged amphipathic α-helix (Figure 2A). The hydrophobic residues of α3 contact the hydrophobic surface of the C-lobe_CaM and the aromatic ring of F925 from α3 inserts into the deep pocket

of C-lobe_CaM (Figure 3C).

The N/C-lobes of CaM bind to TRP CBS1 and CBS2 respectively with high specificity, although the two lobes share very high structural similarities. An analysis of the two structures determined here offers the molecular basis for such binding specificity. Lys75 in the N-lobe of CaM interacts with S838 in CBS1 (Figure 3D1). The residue corresponding to Lys75 in the C-lobe of CaM is the last residue of the proteins and does not form α-helix, which may partly explain why CBS1 prefers to bind to CaM N-lobe. We next modeled the CBS2 peptide onto CaM N-lobe by superimposing the N-lobe and C-lobe structures of CaM shown in Figure 3A. In this modeled structure, Lys924 from CBS2 physically crashes into Lys75 from CaM (Figure 3D2). Thus, CBS2 is unfit to bind to the CaM N-lobe. In line with this analysis, when Lys924 of CBS2 is substituted with Ala, the mutant CBS2 became to be a CaM N-lobe binder (Kd: 7.94±0.88 μM, Figure S2C). Thus, the selectivity of CBS2 for the C-lobe concomitantly determines the binding of CBS1 to the N-lobe of CaM.

Collectively, the structures of the CBS1/N-lobe_CaM and CBS2/C-lobe_CaM complexes, together with our detailed biochemical studies, demonstrate that two discrete fragments in the tail of TRP separated by a flexible linker of >70 residues simultaneously and non-synergistically bind to the two lobes of Ca^{2+}-CaM forming a stable complex with a 1:1 stoichiometry. Amino acid sequence analysis of TRP CBS12 from different insect species revealed that residues involved in the CaM binding are highly conserved (Figure 2A).

We generated a series of CBS1 and CBS2 mutants to validate the structures of their respective complexes with N- and C-lobes of CaM (Figure 3E and Figure S4). We used ITC assays to measure the binding of each of these mutants to CaM. Replacing hydrophobic residues in the α1 helix of CBS1 (F819 and V820 together or L823 alone) with Ala significantly weakened the CBS1/CaM binding (Figure 3E), supporting our structure-based analysis showing the role of α1 in CBS1's binding to

CaM. As expected, replacing hydrophobic residues in the α2 helix of CBS1 with Ala also invariably weakened its binding to CaM (Figure 3E). In particular, when the anchoring F837 and the neighboring I836 were both replaced by Ala, the mutated CBS1 showed no detectable binding to CaM (Figure S4A4). Similarly, replacing the anchoring F925 together with its neighboring M926 with Ala totally abolished CBS2's binding to CaM (Figure S4B4). Finally, the IF836,837AA and FM925,926AA quadruple mutant of CBS12 exhibited no detectable binding to CaM (Figure 3F).

Ca^{2+}-dependent interaction between TRP and CaM

A previous study showed that CaM can interact in the presence or absence of Ca^{2+} with the C-terminal tail of TRP, as well as TRP extracted from *Drosophila* head lysate (Chevesich et al., 1997), a finding that is different from our current *in vitro* study using the TRP tail fragment. It is possible that the full-length TRP may contain additional CaM binding site(s) or that the tail of the channel may adopt a different conformation in the context of the full-length protein thereby having different CaM binding properties from the fragmented tail purified in our *in vitro* study. To resolve this issue, we attempted to purify TRP from *Drosophila* head lysates for CaM binding assay. We took advantage of our previous finding that the NORPA C-terminal domain (NORPA_CT, aa E863-A1095), which contains coiled-coil and PDZ binding motif of the NORPA protein, binds to INAD with a Kd ~10 nM (Ye et al., 2018). Therefore, we used NORPA_CT as an affinity tag to purify the INAD organized INAD/TRP/ePKC complex from *Drosophila* head lysates. We then eluted the INAD associated TRP with a GB1-tagged 15-residue peptide corresponding to the last 15 residues of TRP (TRP_CT, aa R1261-L1275), which was shown to be responsible for the specific interaction between TRP and INAD PDZ3 (Ye et al., 2016). Using this method, we purified sufficient amount of highly homogeneous TRP from *Drosophila* heads for direct CaM binding assays. GST-CaM pull-down assays using the purified TRP from wild-type flies showed that, in the presence of Ca^{2+}, TRP robustly

interacted with CaM (Figure 4A, *left*). Chelating of Ca^{2+} by EDTA totally eliminated the interaction between TRP and CaM (Figure 4A, *left*).

To validate whether the CaM binding sites within CBS12 delineated from our *in vitro* biochemical study are indeed responsible for the TRP/CaM interaction, we compared the binding of CaM to the wild-type full-length TRP (TRP-WT) or to TRP containing the IF836,837AA and FM925,926AA quadruple mutations in CBS12 (Figure 3E). No detectable binding between CaM and TRP with the quadruple mutation purified from transgenic fly heads was observed, either in the presence or absence of Ca^{2+} (Figure 4A, *right*). The complete loss of CaM binding of the quadruple mutant of TRP indicated that CBS12 is solely responsible for TRP to bind to CaM. This result also supports our earlier analysis showing that the CBS-A site corresponding to the connecting helix of the channel (Figure 1) is not likely a functional CaM binding site in the full-length TRP.

Amino acid sequence analysis indicated that the CaM binding tail and the tetramer forming coiled coil domain of TRP are separated by a relatively short stretch of connecting residues (Figures 1F and 2A). We next tested whether CaM binding may promote polymerization of TRP. We created a homotetramer of TRP CBS12 by fusing a tetrameric leucine zipper GCN4 coiled-coil domain (Harbury et al., 1993) to aa 783-940 of TRP, so that the GCN4-CBS12 fusion protein resembles the actual tail assembly mode of the full-length TRP (see Figure 1F&G) (Duan et al., 2018; Tang et al., 2018). The GCN4-CBS12 and Trx-CaM complex could be purified to high homogeneity. AUC sedimentation velocity assay showed that the GCN4-CBS12/Trx-CaM complex formed a single peak with a molecular mass of ~225 kD (Figure 4B), corresponding to a 4:4 molar ratio complex. Negative staining electron microscopy further showed that addition of CaM, either in the apo- or in the Ca^{2+}-saturated forms, to the full-length TRP purified from *Drosophila* heads did not change the oligomerization state of the channels (Figure S5). Thus, CaM binding is not likely to cause multimerization of TRP tetramers via its C-terminal tail.

Combining the above biochemical and structural results, we built an interaction model between TRP C-terminal tail and CaM by modeling the TRP CBS1/N-lobe complex and CBS2/C-lobe complex crystal structures onto the cryo-EM structure of mouse TRPC4 (mTRPC4, PDB: 5Z96) (Duan et al., 2018) (Figure 4C&D). We believe that the most likely mode of the interaction is that each Ca^{2+}-CaM binds to CBS1 and CBS2 with the same subunit of the TRP tetrameric tail (Figure 4C), as we could only detect a stable 1:1 Ca^{2+}-CaM/CBS12 complex in our study (Figure 1D&2C). Since CBS1 and CBS2 are connected by a flexible linker of >70 residues, it is nonetheless possible that the two lobes of CaM may bind to CBS1 and CBS2 from two neighboring TRP tails forming an inter-subunit cross-connected TRP tail assembly (Figure 4D). Further work will be required to differentiate which mode might be adopted by the full-length TRP.

CaM binding to the tail does not directly modulate TRP channel activity under physiological conditions

We next asked whether Ca^{2+}-dependent binding of CaM to the C-terminal tail of TRP plays a role in the channel activity of TRP during phototransduction by recording whole-cell voltage clamped responses to light in photoreceptors from dissociated ommatidia. In photoreceptors expressing wild-type TRP channels brief light flashes delivered in normal bath (containing 1.5 mM Ca^{2+}) elicit rapid responses that peak within ~40 ms and return to baseline after ~100 ms. As previously reported (e.g. Hardie, 1991; Reuss et al, 1997; Henderson et al, 2000) the rapid kinetics are dependent upon sequential positive and negative feedback mediated by Ca^{2+} influx via the TRP channels, and in the absence of extracellular Ca^{2+} (0 Ca^{2+}, 1 mM EGTA) kinetics of both excitation and inactivation are slowed ~10-fold (Figure 5A).

We generated transgenic flies expressing TRP with double Ala substitutions in both CBS1 (IF836,837AA) and CBS2 (FM925,926AA) respectively, as well as a

quadruple mutant of TRP with both CBS1 and CBS2 disrupted. Although our biochemical assays showed that these mutations render CaM binding to TRP undetectable, amplification, rapid kinetics and their dependence upon Ca^{2+} appeared essentially unaffected in any of these mutants (Figure 5A-D, quantified in Figure 5E). These surprising results suggest that the Ca^{2+} dependence of TRP channel activity in phototransduction must be mediated by another mechanism(s). Nevertheless, upon closer inspection, a subtle but consistent phenotype was detected in all three mutants. Thus, whilst light response amplitudes in physiological calcium were similar to those of TRP-WT, in Ca^{2+} free bath they were ~3 times larger than responses observed in TRP-WT under the same conditions (Figure 5A-D, quantified in Figure 5F). It appears that, without Ca^{2+}-CaM restriction, the open probability of TRP somehow can increase. This extracellular Ca^{2+} independent effect of the CBS mutations is not readily understood but may imply some indirect (allosteric) effect of this region on channel open probability. Future studies will be required test this possibility.

TRPC4 binds to Ca^{2+}-CaM with a similar mode as TRP does

Among the TRP subfamilies, TRPCs share the highest sequence similarity to TRP (Montell, 2005; Ramsey et al., 2006). Within the TRPC subfamily, TRPC4 and TRPC5 are most closely related to TRP, and both are also activated by the phospholipase C-mediated signaling cascade. Recently, TRPC3, TRPC4, TRPC5 and TRPC6 cryo-EM structures have been determined (Duan et al., 2018; Duan et al., 2019; Tang et al., 2018), and all of them share similar conformations in their structured regions observable by cryo-EM. Each TRPC channel contains N-terminal ankyrin repeats followed by six transmembrane helices. TRPC C-terminal tails contain a common TRP box, a connecting helix, and a coiled-coil domain, followed by a stretch of disordered sequences with very different lengths (Figure 6A, also see Figure 1F&G). Regrettably, the very C-terminal tails after coiled-coil domain of the TRPC channels are invisible in the cryo-EM structures. Interestingly, previous studies

demonstrated that the C-terminal tail of TRPC4 also contains 2 CBSs (CBS1 aa D785-N812 and CBS2 aa E827-E854 corresponding to the mouse TRPC4 sequence) (Tang et al., 2001; Trost et al., 2001), while TRPC5 only contains 1 CBS (aa K829-S858) (Ordaz et al., 2005). To test whether the Ca^{2+}-CaM interaction mode found in the *Drosophila* TRP tail might have been adopted by mammalian TRPC members, we investigated the binding of CaM to each of the TRPC tails.

First, we assayed the binding of CaM to each member of the TRPC subfamily (Figure 6A) by GST pull down assay. Each of the TRPC tails used for the binding assays contains the coiled-coil domain to the C-terminal end. GST-CaM was used to pull down GFP-TRPC tail expressed in HEK293T cells. This pull-down assay showed that, among the seven TRPC tails, only the TRPC4 and TRPC5 showed positive Ca^{2+}-CaM binding (Figure 6B&C). Analytical gel-filtration coupled with SLS analysis demonstrated that both Trx-TRPC4 tail and Trx-TRPC5 tail formed 1:1 complexes with CaM in a Ca^{2+}-dependent manner (Figure 6D and Figure S8). Detailed mapping using ITC-based quantitative binding analysis revealed that CaM interacts with the first half (CBS1, aa K758-S817) and the second half (CBS2, aa A818-L974) of TRPC4 tail with a K_d values of 0.70±0.06 μM and 1.17±0.22 μM, respectively (Figure 6E and Figure S6). The K_d value of CaM to the entire tail of TRPC4 (aa K758-L974) is 0.34±0.06 μM (Figure 6E), likely due to the mild synergism resulting from the relatively short spacing between CBS1 and CBS2 of TRPC4 (Figure S6A). Interestingly, the mutation eliminating Ca^{2+} binding to the N-lobe (E31/67Q) of CaM abolished its binding to CBS1, and the mutation eliminating Ca^{2+} binding to the C-lobe (E104/140Q) of CaM had very little impact on its binding to CBS1, showing that similar to the *Drosophila* TRP CBS1/N-lobe interaction, CBS1 of TRPC4 also specifically binds to the N-lobe of CaM. However, different from the TRP CBS2/C-lobe_CaM interaction, the direct binding between TRPC4 CBS2 and C-lobe_CaM was too weak to detect. In the absence of CBS1, CBS2 can bind to Ca^{2+}-CaM with a Kd of 1.17±0.22 μM. This binding is also

contributed by the N-lobe of CaM, as elimination of Ca^{2+} binding to the N-lobe of CaM also abolished CBS2/CaM binding (Figure 6E). Based on the above data, we propose that the N-lobe of CaM plays a dominant role in the binding to TRPC4 via CBS1 and the C-lobe plays a minor role in binding to CBS2.

To characterize the molecular mechanism underlying the interaction between TRPC4 and CaM, we tried to determine the structure of TRPC4 CBS12/CaM complex. Although the crystallization of TRPC4 CBS12/CaM complex failed after numerous trials, the crystal structure of the TRPC4 CBS1/N-lobe_CaM complex was determined at a resolution of 1.9 Å (Figure 6F and Table 1). Interestingly, TRPC4 CBS1 in the complex also adopts a "helix-turn-helix" conformation (Figure 6F&G). In the complex, The N-lobe of CaM adopts an open conformation. Both α helices of TRPC4 CBS1 participate in binding to N-lobe_CaM. Different from the TRP CBS1, the α1 of TRPC4 CBS1 is the main helix contacting N-lobe_CaM with L792 serving as the anchoring residue inserting into the deep pocket of N-lobe_CaM (Figure 6F2). Consistent with this structural analysis, substitutions of L792 together with its neighboring F793 with Ala totally abolished TRPC4 CBS1's binding to CaM (Figure S7B).

Using alanine scanning, we were able to show that the hydrophobic residues from TRPC4 CBS2 also contribute to TRPC4's binding to CaM. Replacing the hydrophobic residues in the CBS2 weakened TRPC4 CBS12's binding to CaM by ~3-fold. The combination of the LF792,793AA substitutions in CBS1 and the hydrophobic residue substitutions in CBS2 totally eliminated TRPC4 tail/CaM binding (Figure S7C5&6).

Although the amino acid sequence of *Drosophila* TRP CBS12 is not conserved in TRPC4 and TRPC5 (Figure 6H), *Drosophila* TRP and mammalian TRPC4 still share a similar bidentate CaM interaction mode. In particular, both *Drosophila* TRP CBS1 and mammalian TRPC4 CBS1 form a helix-turn-helix conformation upon binding to CaM N-lobe. It is possible that this bidentate CaM binding mode of *Drosophila* TRP

and mammalian TRPC4 may be a result of evolution. However, since the CaM binding sequences of *Drosophila* TRP and mammalian TRPC4 share very low similarities (Figure 6H), the bidentate CaM binding mode observed for the two channels could be a simple coincidence.

As for the TRPC5 tail, the residues corresponding to the α1 helix in TRPC4 CBS1 do not exist (Figure S8B), and thus the TRPC5 tail may not contain a CaM-binding CBS1 found in TRPC4. However, the residues corresponding to E831-K852 (based on mouse TRPC5 sequence) can be aligned with the sequence of TRPC4 CBS2 (Figure S8B). The TRPC5 tail fragment containing E831-K852 was shown to bind to CaM with a Kd of 1.25±0.32 μM (Figure S8C). Substitution of the hydrophobic residues within E831-K852 (i.e. residues highlighted with blue dots in Figure S8B) totally abolished the binding between TRPC5 tail and CaM. Therefore, TRPC5 should only contains one continuous CaM binding segment spanning E831-K852 and the binding between TRPC5 tail to CaM is about 4 times weaker than the binding between TRPC4 tail and CaM.

DISCUSSION

Previous studies have reported that Ca^{2+} plays both positive feedback and negative feedback regulations on the TRP channel activation and termination processes. However, how Ca^{2+} acts on the TRP channel to regulate channel activity remains to be elucidated. On the other hand, although CaM has been reported to bind to the TRP channel, the molecular mechanism underlying CaM/TRP interaction is not known.

Here, we have elucidated the detailed molecular mechanism underlying the interaction between TRP and CaM. We show that CaM utilizes its two lobes to grasp two CBSs of TRP separated by more than 70 residues in a Ca^{2+}-dependent manner. Upon Ca^{2+}-CaM binding, TRP CBS1 forms a unique “helix-turn-helix” structure

while CBS2 forms a canonical single α helix (Figure 3A). The separation of N- and C-lobe_CaM binding sites by an elongated flexible linker has recently been observed in the cryo-EM structures of TRPV5 and TRPV6 (Dang et al., 2019; Hughes et al., 2018; Singh et al., 2018). However, both CBSs on TRPV5 and TRPV6 form a single amphipathic α helix structure upon CaM binding. In TRPV5 and TRPV6, the distal CBS2-bound C-lobe of Ca^{2+}-CaM functions to block the channel Ca^{2+} conductance by inserting the side chain of trimethylated K115 into the channel pore by forming a highly unusual trimethyllysine/$(Trp)_4$ cation-π cage (Dang et al., 2019; Hughes et al., 2018; Singh et al., 2018; Zhang et al., 1994). This trimethyl lysine/$(Trp)_4$ cation-π cage presumably explains why only Lys115 out of a total of 8 Lys residues in CaM is trimethylated (Roberts et al., 1986; Zhang et al., 1994).

TRP shares greater similarity with the TRPC subfamily channels. TRPC channels include a four-helix bundle formed by the coiled-coil domain after the connecting helix, which functions as a fence separating the channel pore from the rest of the C-terminal tail (Figure 1G). Therefore, the CBS12 bound CaM is unlikely to directly block the channel pore (Figure 4C&D). Additionally, there exists a stretch of flexible sequences of 35-residues connecting the end of the four-helix bundle to the N-terminus of CBS1 in TRPC4 (aa R755-N789) (Duan et al., 2018) (Figure 6H). Similarly, there exists a 33-residue flexible linker between the predicted four-helix bundle and CBS1 in TRP (aa N783-F815) (Figure 4C&D). Thus, we believe that the Ca^{2+}-dependent binding of CaM to the TRP tail (or to TRPC4 tail) is not likely to directly alter the channel pore properties. Indeed, in *Drosophila* eyes, replacing WT TRP with TRP variants containing the CBS1 CaM binding deficient mutation (IF836,837AA), or the CBS2 CaM binding mutation (FM925,926AA), or both CBS1 and CBS2 mutations (the IF836,837AA and FM925,926AA quadruple mutant; characterized in Figure 3D and Figure 4A) did not affect light responses mediated by the channels under physiological conditions. In particular and surprisingly, both the positive and negative feedback mediated by Ca^{2+} appeared fully intact even in the

quadruple mutant, which is incapable of binding Ca^{2+}-CaM (Figure 5). This suggests that Ca^{2+} must mediate its pronounced feedback effects on the channel by a as yet unidentified molecular mechanism. One possibility is that Ca^{2+} may directly, instead of via CaM, bind to and regulate TRP activity. It is also possible that CaM binding to the tail of TRP may be required for the downstream signaling or the INAD-mediated signalplex organization. For example, CaM may shuttle between TRP and other CaM binding proteins in response to light-dependent Ca^{2+} concentration fluctuations in rhabdomere (Porter et al., 1995; Porter et al., 1993). Concentrating CaM within the rhabdomere by several proteins including TRP and NINAC may provide a mechanism for fast Ca^{2+}-dependent signaling in *Drosophila* photoreceptors. Future studies will be required to tease out the physiological role of Ca^{2+}-dependent CaM binding to TRP tail.

In summary, we discovered an unexpected Ca^{2+}-dependent interaction mode between CaM and TRP C-terminal tail. Our biochemical and structural studies of the interaction between CaM and TRP tail reveal the remarkable target binding capacity of CaM. We further showed that CaM can bind to TRPC4 tail with a mode like that between CaM and TRP. The remarkable versatility of CaM in binding to its targets reminds us that CaM, the master Ca^{2+} signal modulator, may bind to and regulate activities of many other ion channels or transmembrane receptors with previously unknown interaction modes.

MATERIALS AND METHODS

Key resources table

Reagent type (species) or resource	Designation	Source or reference	Identifiers
Constructs			
Strain, strain background (E.coli)	BL21(DE3)	Novagen	Cat #69450
Strain, strain background (E.coli)	Rosseta(DE3)	Novagen	Cat #70954
Cell line (human)	HEK293T	ATCC	Cat #CRL-3216; RRID: CVCL_0063
Transfected construct (plasmid)	Flag-*Drosophila* TRP CBS12: aa N783-D940	This paper	NCBI: NM_057420.4
Transfected construct (plasmid)	GFP-TRPC1 Mouse: aa T757-N793	This paper	NCBI: NM_011643.4
Transfected construct (plasmid)	GFP-TRPC2 Mouse: aa D1042-S1172	This paper	NCBI: AF111108.1
Transfected construct (plasmid)	GFP-TRPC3 Mouse: aa N788-E836	This paper	NCBI: FJ207475.1
Transfected construct (plasmid)	GFP-TRPC4 Mouse: aa T732-L974	This paper	NCBI: NM_016984.3
Transfected construct (plasmid)	GFP-TRPC5 Mouse: aa T739-L975	This paper	NCBI: NM_009428.3
Transfected construct (plasmid)	GFP-TRPC6 Mouse: aa N879-R930	This paper	NCBI: NM_013838.2
Transfected construct (plasmid)	GFP-TRPC7 Mouse: aa N805-I862	This paper	NCBI: NM_012035.3
Antibodies			
Antibody	Anti-Flag (M-2) (mouse mAb)	Sigma	Cat #F3165; RRID:AB_259529

Antibody	Anti-Mouse IgG (Goat polyAb)	Sigma	Cat #A4416; RRID: AB_258167
Recombinate Proteins and Synthesized peptides			
Recombinant protein	*Drosophila* Calmodulin: aa A1-K148	This paper	NCBI: NM_078986.3
Recombinant protein	*Drosophila* Calmodulin N_lobe: aa A1-D78	This paper	NCBI: NM_078986.3
Recombinant protein	*Drosophila* Calmodulin C_lobe: T79-K148	This paper	NCBI: NM_078986.3
Recombinant protein	Mouse Calmodulin: aa A1-K148	This paper	NCBI: M19381.1
Recombinant protein	*Drosophila* TRP CBS-AB: aa S717-D940	This paper	NCBI: NM_057420.4
Recombinant protein	*Drosophila* TRP CBS-B: aa N783-D940	This paper	NCBI: NM_057420.4
Recombinant protein	*Drosophila* TRP CBS12: aa N783-D940	This paper	NCBI: NM_057420.4
Recombinant protein	*Drosophila* TRP CBS1: aa T802-K862	This paper	NCBI: NM_057420.4
Recombinant protein	*Drosophila* TRP CBS2: aa M899-D940	This paper	NCBI: NM_057420.4
Recombinant protein	Mouse TRPC4 C-terminal tail: aa K758-L974	This paper	NCBI: NM_016984.3
Recombinant protein	Mouse TRPC4 first half of C-terminal tail: aa K758-S817	This paper	NCBI: NM_016984.3
Recombinant protein	Mouse TRPC4 second half of C-terminal tail: aa A818-L974	This paper	NCBI: NM_016984.3
Recombinant protein	Mouse TRPC5 C-terminal tail: aa K765-L975	This paper	NCBI: NM_009428.3
Recombinant protein	Mouse TRPC5 first half of C-terminal tail: aa K765-S837	This paper	NCBI: NM_009428.3
Recombinant protein	Mouse TRPC5 second half of C-terminal tail: aa G823-L975	This paper	NCBI: NM_009428.3
Synthesized peptide	Mouse TRPC4 CBS1: aa D758-N812	Shenzhen PepBiotic Co., Ltd.	NCBI: NM_016984.3
Synthesized	Mouse TRPC4 CBS2:	Shenzhen	NCBI: NM_016984.3

peptide	aa E827-E854	PepBiotic Co., Ltd.	
Commercial assays and Softwares			
Commercial assay or kit	Clone Express II, One-Step Cloning Kit	Vazyme Biotech Co., Ltd	Cat #C112
Commercial assay or kit	ViaFect transfection reagent	Promega Corporation	Cat #E4981
Software, algorithm	ASTRA6.1	Wyatt Technology Corporation	http://www.wyatt.com/products/software/astra.html
Software, algorithm	Origin7.0	OriginLab	http://www.originlab. com/; RRID: SCR_002815
Software, algorithm	GraphPad Prism	GraphPad Software Inc.	http://www.graphpad.com/scientific-software/prism; RRID: SCR_002798
Software, algorithm	HKL2000	HKL Research Inc.	http://www.hkl-xray.com/
Software, algorithm	CCP4	PMID: 21460441	http://www.ccp4.ac.uk/; RRID: SCR_007255
Software, algorithm	PHENIX	PMID: 20124702	http://www.phenix-online.org/; RRID: SCR_014224
Software, algorithm	Coot	Emsley et al., 2010	https://www2.mrc-lmb.cam.ac.uk/Personal/pemsley/coot/
Software, algorithm	PyMOL	DeLano Scientific LLC	http://www.pymol.org/; RRID: SCR_000305
Software, algorithm	NMRPipe	NIH	https://spin.niddk.nih.gov/NMRPipe/ref/index.html
Software, algorithm	Sparky	UCSF Sparky	https://www.cgl.ucsf.edu/home/sparky/
Deposited Data			
Crystal structure of TRPCBS1/N-lobe_CaM complex	X-ray diffraction	This paper	PDB code: 7CQV
Crystal structure of TRPCBS2/C-lobe_CaM complex	X-ray diffraction	This paper	PDB code: 7CQH
Crystal structure of	X-ray diffraction	This paper	PDB code: 7CQP

TRPC4CBS1/N-lobe_CaM complex			
Crystal structure of chicken Calmodulin	X-ray diffraction	Rupp et al., 1996	PDB code: 1UP5
cryo-EM structure of mouse TRPC4	cryo-EM	Duan et al., 2018	PDB code: 5Z96
cryo-EM structure of TRPC6	cryo-EM	Tang et al., 2018	PDB code: 5YX9

Plasmids, protein expression and purification

Plasmids carrying different fragments and mutants of TRP, TRPCs and CaM were generated by the standard PCR-based method. All mutations were confirmed by DNA sequencing. Recombinant proteins with N-terminal 6x His-tag were expressed in *Escherichia coli* BL21 (DE3) or Rosseta (DE3) cells in LB medium at 16˚C and purified using Ni sepharose 6 fast flow affinity column, followed by size-exclusion and anion exchange chromatography (GE Healthcare). Purified proteins were prepared in 50 mM Tris-HCl (pH 7.5), 100 mM NaCl, 1 mM $CaCl_2$ and 2 mM β-Mercaptoethanol for most of the experiments. Uniformly ^{15}N-labeled samples were prepared by growing bacteria in M9 minimal medium using $^{15}NH_4Cl$ (Cambridge Isotope Laboratories Inc.) as the sole nitrogen source.

Analytical gel filtration chromatography coupled with static light scattering

Molar mass measurements were performed on an AKTA FPLC system (GE Healthcare) coupled with a static light scattering detector (mini-DAWN, Wyatt) and a differential refractive index detector (Optilab, Wyatt). 50 μM protein samples were loaded to a Superdex 200 Increase 10/300 GL column (GE Healthcare) pre-equilibrated by a buffer composed of 50 mM Tris-HCl (pH 7.5), 100 mM NaCl, 1

mM $CaCl_2$ and 2 mM β-Mercaptoethanol.

Analytical ultracentrifugation analysis

Sedimentation equilibrium and sedimentation velocity experiments were performed using a Beckman Proteomelab XL-I ultracentrifuge equipped with Beckman 50Ti rotor. To preform sedimentation equilibrium experiment, TRP CBS12/CaM complex was centrifuged at 16,000 rpm and equilibrated for 72 h at 16,000 rpm at six sector cells with 3 different concentrations (absorption at 280 nm of 0.3, 0.6, and 0.9, respectively), and scans were taken every 8 h for 2 times, 6 h for 4 times and 4 h for 8 times. To preform sedimentation velocity experiment, TRP CBS12/CaM complex was centrifuged at 40,000 rpm and scans were taken for 400 times with intervals of 1 minute at 2 sector cells at absorption at 280 nm of 0.5. GCN4-CBS12/CaM complex was centrifuged at 24,000 rpm and scans were taken for 400 times with intervals of 1 minute at 2 sector cells at absorption at 280 nm of 0.5. All data were calibrated with the buffer as the background. Sedimentation equilibrium and sedimentation velocity data were analyzed using Sedfit and Sedphat programmes (http://www.analyticalultracentrifugation.com/default). Data fitting was performed using a heterogeneous interaction model and with simulated annealing algorithms (Lebowitz et al., 2002).

NMR experiments

NMR samples contained 0.2 mM of Ca^{2+}-CaM or TRP CBS12/Ca^{2+}-CaM complex in 50 mM Tris-HCl (pH 8.0, with 2 mM DTT) in 90% H_2O/10% D_2O. HSQC spectra were acquired at 30°C on a Varian Inova 800-MHz spectrometer equipped with an actively z-gradient shielded triple resonance probe. Backbone resonance assignment of CaM were obtained from previous paper (Mal and Ikura, 2006). Spectra were analyzed using NMRPipe (Delaglio et al., 1995) and Sparky (T.D. Goddard and D.G. Kneller, SPARKY 3, University of California, San Francisco).

Protein crystallography

Crystals of TRP CBS1/N-lobe_CaM complex (2.5 M Ammonium sulfate, 0.1 M BIS-TRIS propane pH 7.0), TRP CBS2/C-lobe_CaM complex (11.4% w/v Polyethyleneglycol 20,000, 150 mM Sodium acetate, 7% v/v Ethyleneglycol, pH 4.5) and TRPC4 CBS1/N-lobe_CaM complex (55.7 % w/v Polyethylene glycol 1,000, 150 mM MES, 2 % v/v 2-Methyl-2,4-pentanediol, pH 6.0) were obtained by sitting-drop vapor-diffusion method at 16ºC. Diffraction data were collected at the Shanghai Synchrotron Radiation Facility (BL17U or BL19U) at 100K. Data were processed and scaled using HKL2000 (Otwinowski and Minor, 1997).

All three complex crystal structures were determined by molecular replacement with the model of N-lobe_CaM (PDB: 1UP5, Rupp, 1996) using PHASER (McCoy et al., 2007). Furhter manual model building and refinement of the structures were completed iteratively using Coot (Emsley et al., 2010) and PHENIX (Adams et al., 2010). The final models were validated by MolProbity and the statistics are summarized in Table 1. All structure figures were prepared with PyMOL (http://www.pymol.org).

Isothermal titration calorimetry assay

ITC experiments were performed on a MicroCal ITC200 calorimeter (Malvern, UK) at 25˚C. Proteins with high concentrations (300 μM in the TRP cases or 400 μM in the TRPC cases) were loaded into the syringe and titrated into the cells containing corresponding interactors with low concentrations (30 μM in the TRP cases or 40 μM in the TRPC cases). The sample in the syringe was subsequently injected into the cell with a time interval of 120 s (0.5 μl for the first injection and 2 μl each for the following 18 injections). Titration data were analyzed using the Origin7.0 software and fitted with the one-site binding model. The ITC experiments were performed by 3 independent repeats.

GST pull down assay

GST-tagged CaM or GST alone was incubated with purified endogenous TRP or

HEK293T cell lysates expressing Flag-tagged target proteins for 1 h in 4˚C. The mixture was mixed with 20 μl Glutathione Sepharose 4B beads (GE Healthcare) slurry in TBS with 1 mM $CaCl_2$ or 1 mM EDTA for 30 min in 4˚C. After washing twice, the proteins captured by the beads were eluted by boiling with SDS-PAGE loading buffer, resolved by SDS-PAGE and detected using Coomassie brilliant blue R250 staining or Western blot.

Transgenic *Drosophila* expressing mutated TRP

Mutations of "IF836,837AA", "FM925,926AA" and "IF836,837AA & FM925,926AA" were individually introduced into a 6.5-kb *trp* genomic DNA (Montell et al, 1985), and further cloned into the pattB vector. Three corresponding transgenic lines were generated by PhiC31 integrase-mediated transgenesis to insert at the attp40 site (BestGene), and these transgenes were individually recombined into $trpl^{MB10553}$ and $trp^{MB03672}$ double null mutant background. Homozygote with two transgene copies of each TRP variant were analyzed for whole-cell patch clamp recordings and calmodulin binding.

***Drosophila* head preparation and endogenous TRP purification**

Wild type or mutant *Drosophila* were first quick-frozen in liquid nitrogen and shaken hard to break heads from bodies. Then the heads were filtrated by sieves and mechanically crashed and extracted in extraction buffer (v/v, 1:10) containing 50 mM Tris-HCl pH 8.0, 150 mM NaCl, 6 mM (0.3%) n-dodecyl-β-D-maltoside (DDM), 1x cocktail protease inhibitor (Roche). After extraction, the mixture was centrifuged at 14,000 g for 10 min followed by 100,000 g for 45 min at 4˚C. Total protein concentrations of supernatant (about 4 mg/ml) were determined by BCA protein assay. The supernatant was then used in the 3xStrep-NORPA_CT (aa E863-A1095) pull-down assays (similar procedure with the GST pull down assay). After the enrichment of INAD/ePKC/TRP complex by 3xStrep-NORPA to Streptavidin beads (GE Healthcare), TRP were competed from INAD complex by adding excessive

amount of GB1-TRP_CT (aa R1261-L1275) protein. The TRP elution was used for further GST-CaM pull down assay and Transmission Electron Microscopy (TEM) experiments.

Transmission Electron Microscopy

Determination of the polymeric state of endogenous TRP/CaM complex was achieved by negative-staining TEM. Purified endogenous TRP was eluted as a tetramer in Superose 6 Increase 10/300 GL column (GE Healthcare) in the buffer containing 50 mM Tris-HCl pH 8.0, 150 mM NaCl, 0.03% DDM, 2 mM DTT. 4 μL diluted (about 0.01 mg/ml) TRP or TRP/CaM complex (1:1 molar ratio) sample was spotted to glow-discharged carbon-coated copper grids (Beijing Zhongkejingyi Technology). After 60s of absorption, the sample was blotted, and then stained with 2% uranyl acetate. Images were recorded using a transmission electron microscope TEM HT7700 (HITACHI) equipped with a field emission gun and operated at an acceleration voltage of 100 kV.

Cell culture and transfection

HEK293T cells were cultured in Dulbecco's Modified Eagle Medium (DMEM) supplemented with 10% fetal bovine serum (FBS), and 1% of penicillin-streptomycin at 37˚C with 5% CO_2. HEK293T cells were transfected with Flag-tagged target proteins using ViaFect Transfection Reagent (Promega, Madison, WI) following the manufacturer's instruction. After 24-36 h, cells were harvested and stored at -80˚C preparing for the pull-down assay.

Whole-cell patch clamp recordings

Whole-cell patch clamp recordings of photoreceptors from dissociated ommatidia from newly eclosed adult flies of either sex were performed as previously described (e.g. Reuss et al 1997). Standard bath contained (in mM): 120 NaCl, 5 KCl, 10 *N*-Tris-(hydroxymethyl)-methyl-2-amino-ethanesulphonic acid (TES), 4 $MgCl_2$, 1.5 $CaCl_2$, 25 proline and 5 alanine, pH 7.15. For Ca^{2+} free bath $CaCl_2$ was omitted and 1

mM Na_2EGTA added; the solution being applied locally from a nearby puffer pipette. The intracellular pipette solution was (in mM): 140 K gluconate, 10 TES, 4 Mg-ATP, 2 $MgCl_2$, 1 NAD and 0.4 Na-GTP, pH 7.15. Chemicals were obtained from Sigma-Merck (Germany) and VWR (USA). Recordings were made at room temperature (22 ± 1° C) at –70 mV using electrodes of resistance 10-15 MΩ. Data were collected and analyzed using Axon amplifiers and pCLAMP v.9 or 10 software (Molecular Devices, Union City, CA). Photoreceptors were stimulated via a green (522 nm) ultrabright light-emitting-diode (LED) controlled by a custom-made LED driver; intensities were calibrated in terms of effectively absorbed photons by counting quantum bumps at low intensities. Differences between experimental groups were tested with one-way Anova followed by the Tukey's test.

Quantification and Statistical Analysis

Statistical parameters including the definitions and exact values of n (e.g., number of experiments), distributions and deviations are reported in the Figures and corresponding Figure Legends. For TRP channel amplitudes recordings, the results were expressed as mean ± SD using one-way Anova with the Turky’s test.

Acknowledgments

We thank the Shanghai Synchrotron Radiation Facility (SSRF) BL17U1 and BL19U1 for X-ray beam time and the School of Life Science at SUSTech for access of electron microscope. National Key R&D Program of China (2019YFA0508402), Natural Science Foundation of Guangdong Province (2016A030312016) and Shenzhen Basic Research Grant (JCYJ20160229153100269) to M.Z., grants from the National Natural Science Foundation of China (No. 31670765 and 31870746) and Shenzhen Basic Research Grants (JCYJ20170411090807530) to W.L., and a grant from the National Eye Institute (EY010852) to C.M. Grants from and Biological

Sciences Research Council (BB/M007006/1) to RCH) and European Union's Horizon 2020 research and innovation programme (658818-FLYghtCaRE) to RCH and SA. M.Z. is a Kerry Holdings Professor in Science at HKUST.

Author contributions

WC and Z Sun performed biochemical experiments; Z Shen and FY were responsible for structural studies; SA performed electrophysiology experiments, ZC generated transgenic flies; CM, RH, WL, MZ designed and supervised the research, all authors analyzed the data; WC and MZ wrote the manuscript with input from all other authors. MZ coordinated the research.

Competing interests

The authors declare no competing interests.

REFERENCES

Adams, P.D., Afonine, P.V., Bunkoczi, G., Chen, V.B., Davis, I.W., Echols, N., Headd, J.J., Hung, L.W., Kapral, G.J., Grosse-Kunstleve, R.W., *et al.* (2010). PHENIX: a comprehensive Python-based system for macromolecular structure solution. Acta Crystallogr D Biol Crystallogr *66*, 213-221.

Chang, A., Abderemane-Ali, F., Hura, G.L., Rossen, N.D., Gate, R.E., and Minor, D.L., Jr. (2018). A Calmodulin C-Lobe Ca(2+)-Dependent Switch Governs Kv7 Channel Function. Neuron *97*, 836-852 e836.

Chevesich, J., Kreuz, A.J., and Montell, C. (1997). Requirement for the PDZ domain protein, INAD, for localization of the TRP store-operated channel to a signaling complex. Neuron *18*, 95-105.

Chu, B., Liu, C.H., Sengupta, S., Gupta, A., Raghu, P., and Hardie, R.C. (2013). Common mechanisms regulating dark noise and quantum bump amplification in Drosophila photoreceptors. J Neurophysiol *109*, 2044-2055.

Clapham, D.E. (2003). TRP channels as cellular sensors. Nature *426*, 517-524.

Cosens, D.J., and Manning, A. (1969). Abnormal electroretinogram from a Drosophila mutant. Nature *224*, 285-287.

Dang, S., van Goor, M.K., Asarnow, D., Wang, Y., Julius, D., Cheng, Y., and van der Wijst, J. (2019). Structural insight into TRPV5 channel function and modulation. Proc Natl Acad Sci U S A *116*, 8869-8878.

Delaglio, F., Grzesiek, S., Vuister, G.W., Zhu, G., Pfeifer, J., and Bax, A. (1995). NMRPipe: a multidimensional spectral processing system based on UNIX pipes. J Biomol NMR *6*, 277-293.

Duan, J., Li, J., Zeng, B., Chen, G.L., Peng, X., Zhang, Y., Wang, J., Clapham, D.E., Li, Z., and Zhang, J. (2018). Structure of the mouse TRPC4 ion channel. Nat Commun *9*, 3102.

Duan, J.J., Li, J., Chen, G.L., Ge, Y., Liu, J.Y., Xie, K.C., Peng, X.G., Zhou, W., Zhong, J.N., Zhang, Y.X., *et al.* (2019). Cryo-EM structure of TRPC5 at 2.8-angstrom resolution reveals unique and conserved structural elements essential for channel function. Science Advances *5*.

Emsley, P., Lohkamp, B., Scott, W.G., and Cowtan, K. (2010). Features and development of Coot. Acta Crystallogr D Biol Crystallogr 66, 486-501.

Gu, Y., Oberwinkler, J., Postma, M., and Hardie, R.C. (2005). Mechanisms of light adaptation in Drosophila photoreceptors. Curr Biol 15, 1228-1234.

Harbury, P.B., Zhang, T., Kim, P.S., and Alber, T. (1993). A switch between two-, three-, and four-stranded coiled coils in GCN4 leucine zipper mutants. Science (New York, N.Y.) 262, 1401-1407.

Hardie, R.C. (1991). Whole-cell recordings of the light induced current in dissociated Drosophila photoreceptors: evidence for feedback by calcium permeating the light-sensitive channels. Proceedings of the Royal Society of London. Series B: Biological Sciences 245, 203-210.

Hardie, R.C. (1995). Photolysis of caged Ca2+ facilitates and inactivates but does not directly excite light-sensitive channels in Drosophila photoreceptors. The Journal of neuroscience : the official journal of the Society for Neuroscience 15, 889-902.

Hardie, R.C., and Minke, B. (1992). The Trp Gene Is Essential for a Light-Activated Ca2+ Channel in Drosophila Photoreceptors. Neuron *8*, 643-651.

Hardie, R.C., and Raghu, P. (2001). Visual transduction in Drosophila. Nature *413*, 186-193.

Henderson, S.R., Reuss, H., and Hardie, R.C. (2000). Single photon responses in Drosophila photoreceptors and their regulation by Ca2+. J Physiol *524 Pt 1*, 179-194.

Herzog, R.I., Liu, C., Waxman, S.G., and Cummins, T.R. (2003). Calmodulin Binds to the C Terminus of Sodium Channels Nav1.4 and Nav1.6 and Differentially Modulates Their Functional Properties. The Journal of Neuroscience *23*, 8261.

Hoeflich, K.P., and Ikura, M. (2002). Calmodulin in action: diversity in target recognition and activation mechanisms. Cell *108*, 739-742.

Hughes, T.E.T., Pumroy, R.A., Yazici, A.T., Kasimova, M.A., Fluck, E.C., Huynh, K.W., Samanta, A., Molugu, S.K., Zhou, Z.H., Carnevale, V., *et al.* (2018). Structural insights on TRPV5 gating by endogenous modulators. Nat Commun *9*, 4198.

Katz, B., and Minke, B. (2012). Phospholipase C-mediated suppression of dark noise enables single-photon detection in Drosophila photoreceptors. J Neurosci *32*, 2722-2733.

Lebowitz, J., Lewis, M.S., and Schuck, P. (2002). Modern analytical ultracentrifugation in protein science: a tutorial review. Protein Sci *11*, 2067-2079.

Li, H. (2017). TRP Channel Classification. Adv Exp Med Biol 976, 1-8.

Liu, C.H., Satoh, A.K., Postma, M., Huang, J., Ready, D.F., and Hardie, R.C. (2008). Ca2+-dependent metarhodopsin inactivation mediated by calmodulin and NINAC

myosin III. Neuron 59, 778-789.

Mal, T.K., and Ikura, M. (2006). NMR Investigation of Calmodulin. In Modern Magnetic Resonance, G.A. Webb, ed. (Dordrecht: Springer Netherlands), pp. 503-516.

McCoy, A.J., Grosse-Kunstleve, R.W., Adams, P.D., Winn, M.D., Storoni, L.C., and Read, R.J. (2007). Phaser crystallographic software. J Appl Crystallogr *40*, 658-674.

Minke, B., and Selinger, Z. (1996). The roles of trp and calcium in regulating photoreceptor function in Drosophila. Current opinion in neurobiology *6*, 459-466.

Montell, C. (2005). The TRP superfamily of cation channels. Sci STKE *2005*, re3-re3.

Montell, C. (2012). Drosophila visual transduction. Trends in neurosciences *35*, 356-363.

Montell, C., and Rubin, G.M. (1989). Molecular characterization of the Drosophila trp locus: a putative integral membrane protein required for phototransduction. Neuron *2*, 1313-1323.

Montell, C., Jones, K., Hafen, E., and Rubin, G.M. (1985) Rescue of the Drosophila phototransduction mutation trp by germline transformation Science *230*, 1040-1043.

Ordaz, B., Tang, J., Xiao, R., Salgado, A., Sampieri, A., Zhu, M.X., and Vaca, L. (2005). Calmodulin and calcium interplay in the modulation of TRPC5 channel activity. Identification of a novel C-terminal domain for calcium/calmodulin-mediated facilitation. The Journal of biological chemistry *280*, 30788-30796.

Otsuguro, K., Tang, J., Tang, Y., Xiao, R., Freichel, M., Tsvilovskyy, V., Ito, S., Flockerzi, V., Zhu, M.X., and Zholos, A.V. (2008). Isoform-specific inhibition of TRPC4 channel by phosphatidylinositol 4,5-bisphosphate. The Journal of biological chemistry *283*, 10026-10036.

Otwinowski, Z., and Minor, W. (1997). Processing of X-ray diffraction data collected in oscillation mode. Method Enzymol *276*, 307-326.

Porter, J.A., Minke, B., and Montell, C. (1995). Calmodulin binding to Drosophila NinaC required for termination of phototransduction. EMBO J 14, 4450-4459.

Porter, J.A., Yu, M., Doberstein, S.K., Pollard, T.D., and Montell, C. (1993). Dependence of calmodulin localization in the retina on the NINAC unconventional myosin. Science 262, 1038-1042.

Qin, N., Olcese, R., Bransby, M., Lin, T., and Birnbaumer, L. (1999). Ca2+-induced inhibition of the cardiac Ca2+ channel depends on calmodulin. Proc Natl Acad Sci U S A *96*, 2435-2438.

Ramsey, I.S., Delling, M., and Clapham, D.E. (2006). An introduction to TRP channels. Annu Rev Physiol *68*, 619-647.

Reuss, H., Mojet, M.H., Chyb, S., and Hardie, R.C. (1997). In vivo analysis of the drosophila light-sensitive channels, TRP and TRPL. Neuron *19*, 1249-1259.

Roberts, D.M., Rowe, P.M., Siegel, F.L., Lukas, T.J., and Watterson, D.M. (1986). Trimethyllysine and protein function. Effect of methylation and mutagenesis of lysine 115 of calmodulin on NAD kinase activation. The Journal of biological chemistry *261*, 1491-1494.

Rupp, B., Marshak, D. R., & Parkin, S. (1996). Crystallization and preliminary X-ray analysis of two new crystal forms of calmodulin. Acta Crystallographica Section D: Biological Crystallography, 52(2), 411-413.

Scott, K., Sun, Y., Beckingham, K., and Zuker, C.S. (1997). Calmodulin regulation of Drosophila light-activated channels and receptor function mediates termination of the light response in vivo. Cell *91*, 375-383.

Singh, A.K., McGoldrick, L.L., Twomey, E.C., and Sobolevsky, A.I. (2018). Mechanism of calmodulin inactivation of the calcium-selective TRP channel TRPV6. Sci Adv *4*, eaau6088.

Sun, Z., Zheng, Y., and Liu, W. (2018). Identification and characterization of a novel calmodulin binding site in Drosophila TRP C-terminus. Biochem Biophys Res Commun *501*, 434-439.

Suss-Toby, E., Selinger, Z., and Minke, B. (1991). Lanthanum reduces the excitation efficiency in fly photoreceptors. The Journal of general physiology *98*, 849-868.

Tang, J., Lin, Y., Zhang, Z., Tikunova, S., Birnbaumer, L., and Zhu, M.X. (2001). Identification of common binding sites for calmodulin and inositol 1,4,5-trisphosphate receptors on the carboxyl termini of trp channels. The Journal of biological chemistry *276*, 21303-21310.

Tang, Q., Guo, W., Zheng, L., Wu, J.X., Liu, M., Zhou, X., Zhang, X., and Chen, L. (2018). Structure of the receptor-activated human TRPC6 and TRPC3 ion channels. Cell Res 28, 746-755.

Tidow, H., and Nissen, P. (2013). Structural diversity of calmodulin binding to its target sites. FEBS J 280, 5551-5565.

Trost, C., Bergs, H., Himmerkus, N., and Flockerzi, V. (2001). The transient receptor potential, TRP4, cation channel is a novel member of the family of calmodulin binding proteins. Biochem J *355*, 663-670.

Tsunoda, S., Sierralta, J., Sun, Y., Bodner, R., Suzuki, E., Becker, A., Socolich, M., and Zuker, C.S. (1997). A multivalent PDZ-domain protein assembles signalling complexes in a G-protein-coupled cascade. Nature *388*, 243-249.

Wang, L., Fu, T.M., Zhou, Y., Xia, S., Greka, A., and Wu, H. (2018). Structures and gating mechanism of human TRPM2. Science *362*.

Yap, K.L., Kim, J., Truong, K., Sherman, M., Yuan, T., and Ikura, M. (2000). Calmodulin target database. J Struct Funct Genomics 1, 8-14.

Ye, F., Huang, Y., Li, J., Ma, Y., Xie, C., Liu, Z., Deng, X., Wan, J., Xue, T., Liu, W., et al. (2018). An unexpected INAD PDZ tandem-mediated plcbeta binding in Drosophila photo receptors. Elife 7.

Ye, F., Liu, W., Shang, Y., and Zhang, M. (2016). An Exquisitely Specific PDZ/Target Recognition Revealed by the Structure of INAD PDZ3 in Complex with TRP Channel Tail. Structure *24*, 383-391.

Yin, Y., Le, S.C., Hsu, A.L., Borgnia, M.J., Yang, H., and Lee, S.Y. (2019). Structural basis of cooling agent and lipid sensing by the cold-activated TRPM8 channel. Science *363*.

Zhang, M., Abrams, C., Wang, L., Gizzi, A., He, L., Lin, R., Chen, Y., Loll, P.J., Pascal, J.M., and Zhang, J.F. (2012). Structural basis for calmodulin as a dynamic calcium sensor. Structure *20*, 911-923.

Zhang, M., Huque, E., and Vogel, H.J. (1994). Characterization of trimethyllysine 115 in calmodulin by 14N and 13C NMR spectroscopy. The Journal of biological chemistry *269*, 5099-5105.

Zhang, M., Tanaka, T., and Ikura, M. (1995). Calcium-induced conformational transition revealed by the solution structure of apo calmodulin. Nat Struct Biol *2*, 758-767.

Zhu, M.X. (2005). Multiple roles of calmodulin and other Ca(2+)-binding proteins in the functional regulation of TRP channels. Pflugers Archiv : European journal of physiology *451*, 105-115.

Table 1: Statistics of X-ray Crystallographic Data Collection and Model Refinement

Data Collection			
Dataset	TRP CBS1/N-lobe	TRP CBS2/C-lobe	TRPC4 CBS1/N-lobe
Space group	$H3_2$	$I4_1$	$P6_122$
Wavelength	0.97890	0.97890	0.97890
Unit cell (a,b,c,Å)	98.449, 98.449, 134.26	58.344, 58.344, 92.21	64.46, 46.46, 120.75
Unit cell (α,β,γ,˚)	90, 90, 120	90, 90, 90	90, 90, 120
Resolution range (Å)	49.27-1.78(1.81-1.78)	49.31-2.15(2.19-2.15)	50.00-1.90(1.97-1.90)
No. of unique reflections	24105(1192)	8342(369)	12754(1169)
Redundancy	19.6(19.5)	12.6(9.1)	7.4(7.5)
I/sigma	55.8(7.27)	50.18(2.71)	19.11(2.29)
Completeness (%)	100.0(100.0)	99.1(88.5)	99.7(99.5)
Rmerge[a] (%)	6.1(35.6)	5.0(36.8)	10.2(100)
Structure Refinement			
Resolution (Å)	49.27-1.78(1.85-1.78)	49.31-2.15(2.19-2.15)	50.00-1.90(2.09-1.90)
R_{cryst}[b]/R_{free}[c](%)	20.48/23.39	21.40/25.32	21.94/24.98
Rmsd bonds (Å) /angles (˚)	0.007/0.963	0.0107/1.45	0.006/0.909
Average B factors ($Å^2$)	30.88	68.58	27.54
No. of atoms			
Protein atoms	1444	664	725
Water	73	0	30
Other molecules	4	2	2
No. of reflections			
Working set	22889(2530)	7910(513)	11637(2800)
Test set	1202(127)	415(34)	607(140)
Ramachandran plot regions			
Favored(%)	98.40	98.85	98.90
Allowed(%)	0.53	0.00	1.10
Outliers(%)	0.53	1.15	0.00

Numbers in parentheses represent the value for the highest resolution shell.

a. $R_{merge} = \Sigma |I_i - \langle I \rangle| / \Sigma I_i$, where I_i is the intensity of measured reflection and $\langle I \rangle$ is the mean intensity of all symmetry-related reflections.

b. $R_{cryst}=\Sigma||F_{calc}| - |F_{obs}||/\Sigma F_{obs}$, where F_{obs} and F_{calc} are observed and calculated structure factors.

c. $R_{free}= \Sigma T||F_{calc}| - |F_{obs}||/\Sigma F_{obs}$, where T is a test data set of about 5% of the total unique reflections randomly chosen and set aside prior to refinement.

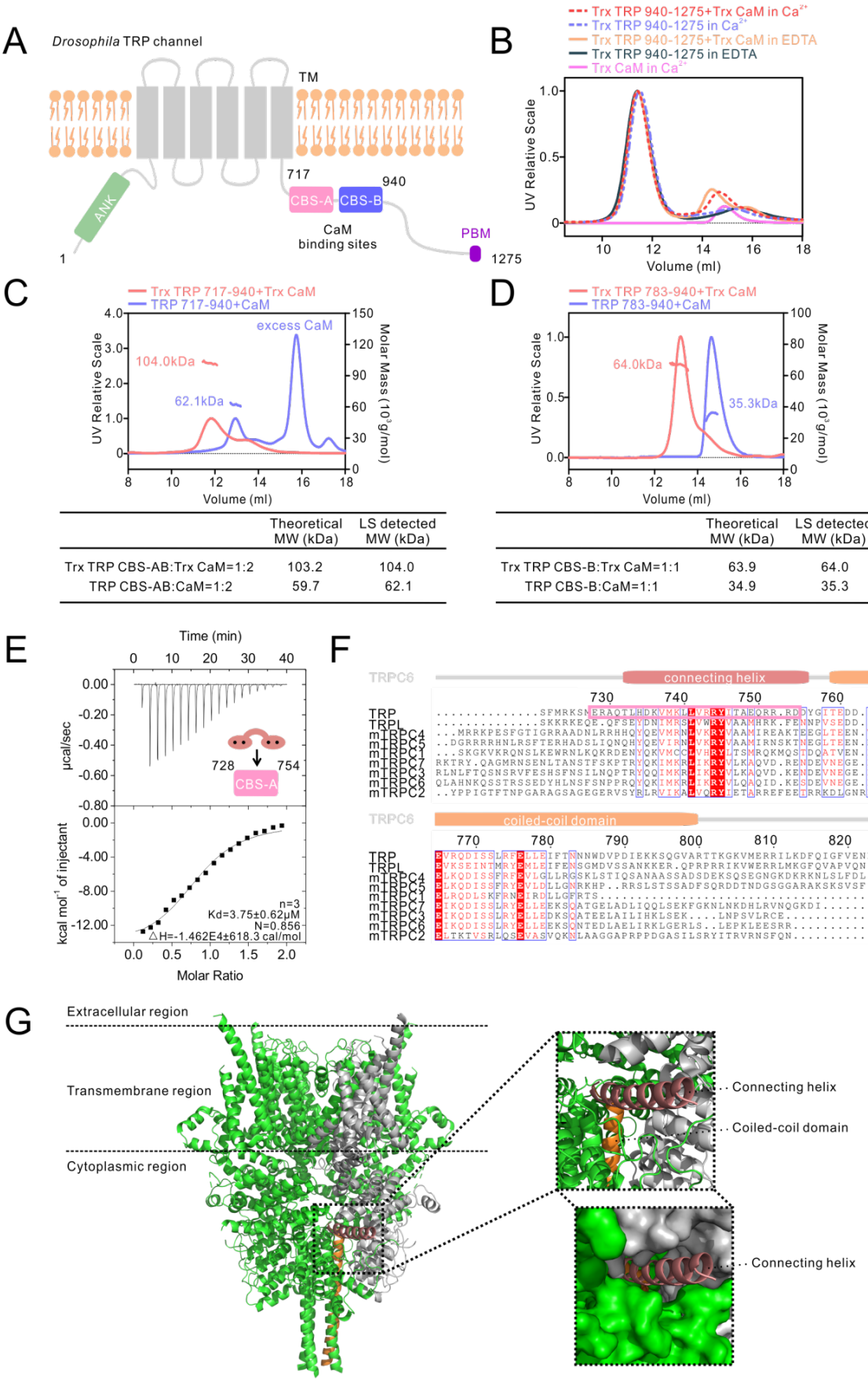

	Theoretical MW (kDa)	LS detected MW (kDa)
Trx TRP CBS-AB:Trx CaM=1:2	103.2	104.0
TRP CBS-AB:CaM=1:2	59.7	62.1

	Theoretical MW (kDa)	LS detected MW (kDa)
Trx TRP CBS-B:Trx CaM=1:1	63.9	64.0
TRP CBS-B:CaM=1:1	34.9	35.3

Figure 1: Identification of CaM binding sites at the *Drosophila* TRP C-terminal Tail

(A) Schematic diagrams showing the domain and topographic organizations of *Drosophila* TRP channel. The two CaM binding sites are designated as CBS-A and CBS-B. ANK stands for ankyrin repeats and PBM represents PDZ domain binding motif.

(B) Analytical gel filtration chromatography analysis showing that there is no detectable binding between TRP (940-1275) and CaM both in the presence and absence of Ca^{2+}.

(C) Analytical gel filtration chromatography coupled with static light scattering analysis showing that TRP CBS-AB (717-940), with or without the Trx-tag, binds to Ca^{2+}-CaM forming a 1:2 molar ratio complex.

(D) Analytical gel filtration chromatography coupled with static light scattering analysis showing that TRP CBS-B (783-940), with or without the Trx-tag, binds to Ca^{2+}-CaM forming a 1:1 molar ratio complex.

(E) Isothermal titration calorimetry (ITC)-based measurement of the binding of Ca^{2+}-CaM to the TRP CBS-A peptide (728-754).

(F) Sequence alignment of the connecting helix and the coiled-coil domain of TRP, TRPL and mouse TRPC1-7. Based on the cryo-EM structure of TRPC6, the connecting helix is shown as a bar in salmon and the coiled-coil domain is indicated as an orange bar above the alignment. The CBS-A peptide of TRP used in panel E is indicated by a pink box.

(G) Ribbon diagram representation of the close state cryo-EM structure of TRPC6 (PDB: 5YX9). The region highlighted in the dashed box contains the connecting helix (colored in salmon) and the coiled coil domain (colored in orange) of TRPC6. For simplicity, only one monomer subunit of the connecting helix and the coiled coil domain are colored in both the ribbon and ribbon combined with the surface model shown on the right (the rest part colored in gray). The other three monomer subunits are colored in green. The structure shows that the connecting helix is completely embedded in the tetramer structure of TRPC6 and not accessible to CaM.

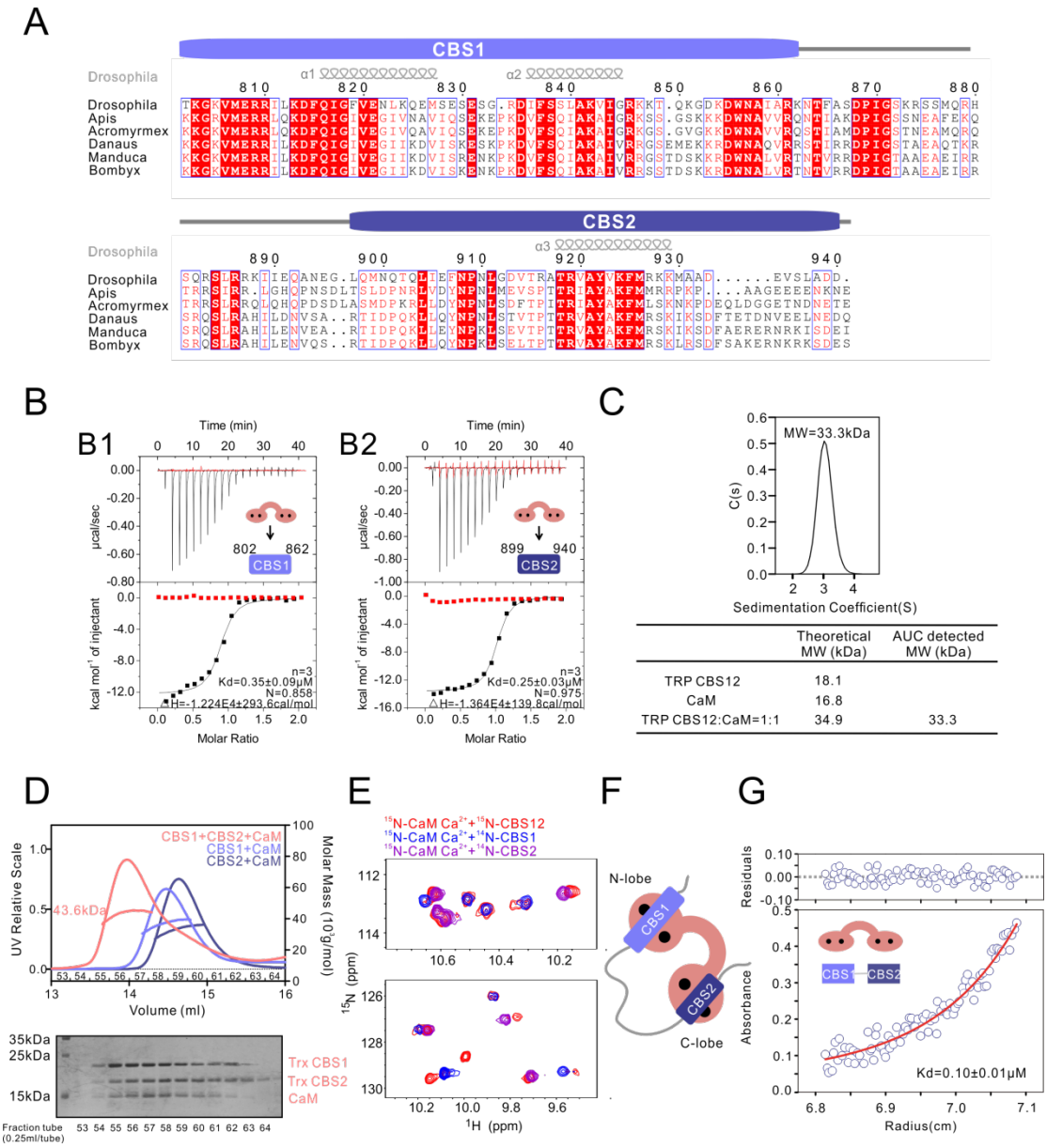

Figure 2: CaM binds to TRP C-terminal tail with an unexpected binding mode

(A) Sequence alignment of TRP CBS-B from different insect species. The two CaM binding sites, CBS1(802-862) and CBS2(899-940), are highlighted and their secondary structures when in complex with Ca^{2+}-CaM are indicated. In this alignment, the completely conserved residues are shaded in red, highly conserved residues shown in red, and non-conserved residues in black.

(B) ITC-based measurements of the bindings of CaM to TRP CBS1 (B1) and CBS2 (B2) in the presence (black curve) or absence (red curve) of Ca^{2+}.

(C) Analytical ultracentrifugation sedimentation velocity analysis showing that Ca^{2+}-CaM binds to TRP CBS12 forming a homogenous 1:1 molar ratio complex.

(D) Analytical gel filtration coupled with static light scattering showing that CBS1, CBS2 and CaM can form a stable ternary complex with a 1:1:1 stoichiometry. The SDS-PAGE with Coomassie blue staining at the bottom panel shows the protein composition of the elution peak of the CBS1, CBS2 and CaM mixture shown in red at the top panel.

(E) Overlay of the $^{1}H,^{15}N$-HSQC spectra of the ^{15}N-Ca^{2+}-CaM/^{15}N-CBS12 complex (red) with those of ^{15}N-Ca^{2+}-CaM in complex with ^{14}N-CBS1 (blue) and ^{14}N-CBS2 (purple), respectively.

(F) Cartoon showing the binding mode between TRP CBS12 and Ca^{2+}-CaM.

(G) Dissociation constants of the TRP CBS12/Ca^{2+}-CaM complex derived from the analytical ultracentrifugation sedimentation equilibrium analysis.

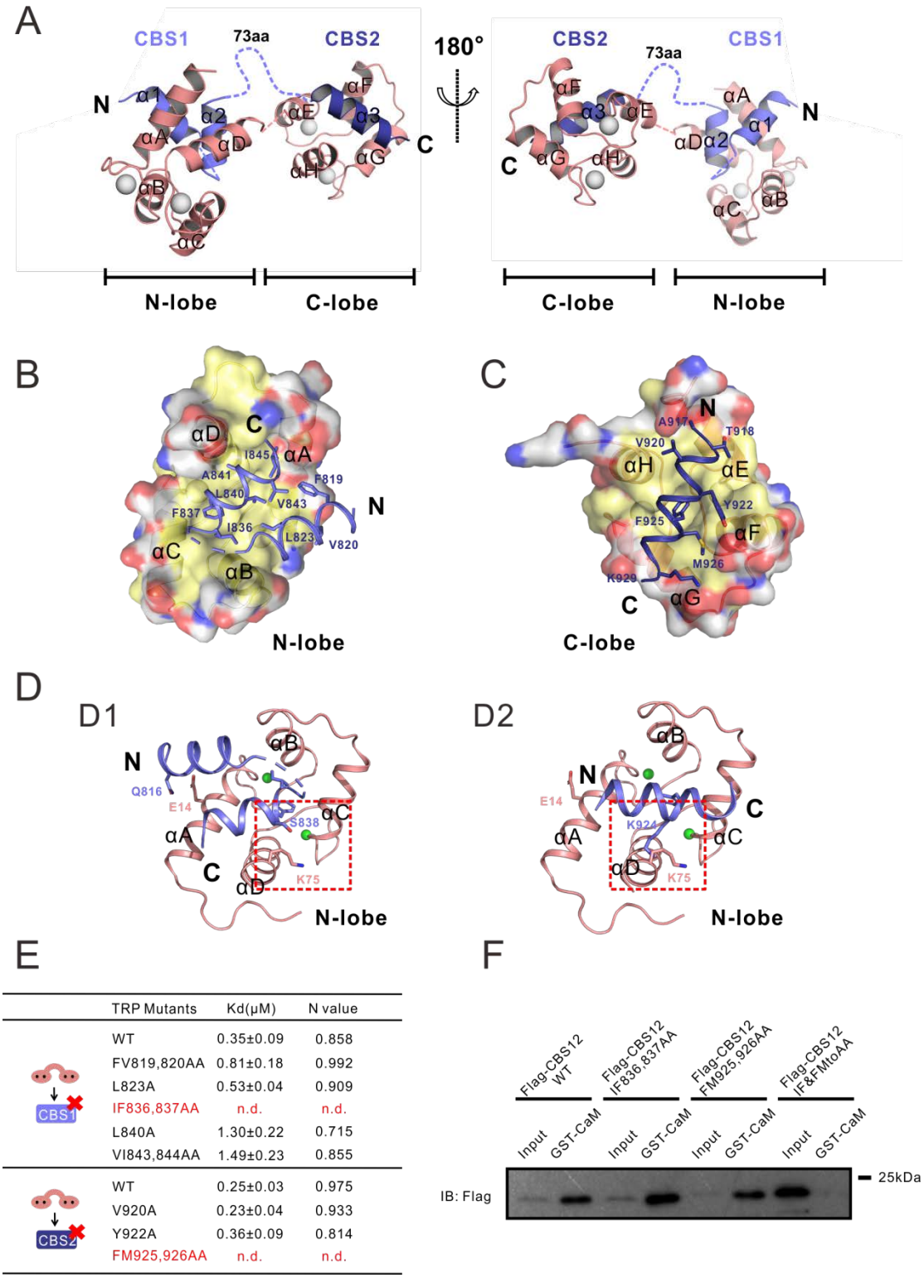

	TRP Mutants	Kd(μM)	N value
CBS1	WT	0.35±0.09	0.858
	FV819,820AA	0.81±0.18	0.992
	L823A	0.53±0.04	0.909
	IF836,837AA	n.d.	n.d.
	L840A	1.30±0.22	0.715
	VI843,844AA	1.49±0.23	0.855
CBS2	WT	0.25±0.03	0.975
	V920A	0.23±0.04	0.933
	Y922A	0.36±0.09	0.814
	FM925,926AA	n.d.	n.d.

Figure 3: Crystal structures of Ca^{2+}-CaM in complex with TRP CBS1 and CBS2 and validation of the structure

(A) Ribbon diagrams showing the structures of the TRP CBS1/N-lobe_CaM complex and the CBS2/C-lobe_CaM complex. The N/C-lobe_CaM are colored in salmon. TRP CBS1 is colored in pale blue, and the CBS2 is colored in deep blue. The two

lobes of CaM are arbitrarily connected with a dotted line. CBS1 and CBS2 in the complex are separated by a 73-residues linker indicated by a dashed line.

(B,C) The combined surface (N/C-lobe_CaM) and ribbon (TRP CBS1/CBS2) models showing the interaction between TRP CBS1/CBS2 and Ca^{2+}-CaM. In the surface model, the positively charged amino acids of N/C-lobe_CaM are highlighted in blue, the negatively charged residues in red, the hydrophobic residues in yellow, and the others in white. The sidechains of residues from TRP CBS1/CBS2 that are involved in binding to CaM are shown with the stick model.

(D) The ribbon models of the original structure of CBS1/N-lobe complex (D1) and the aligned structure of CBS2/N-lobe complex (D2). The critical K75 from the CaM N-lobe are highlighted by red dashed box.

(E) Table summarizing the binding affinities of various mutants of CBS1 and CBS2 to Ca^{2+}-CaM derived from ITC-based assays.

(F) GST pull-down assay showing that when both IF836,837AA and FM925,926AA are introduced into TRP-CBS12, the interaction between CBS12 and CaM is totally abolished. Note that we intentionally used excess amount of the IF836,837AA/FM925,926AA quadruple mutant in the pull-down assay to show that even weak interaction could not be detected.

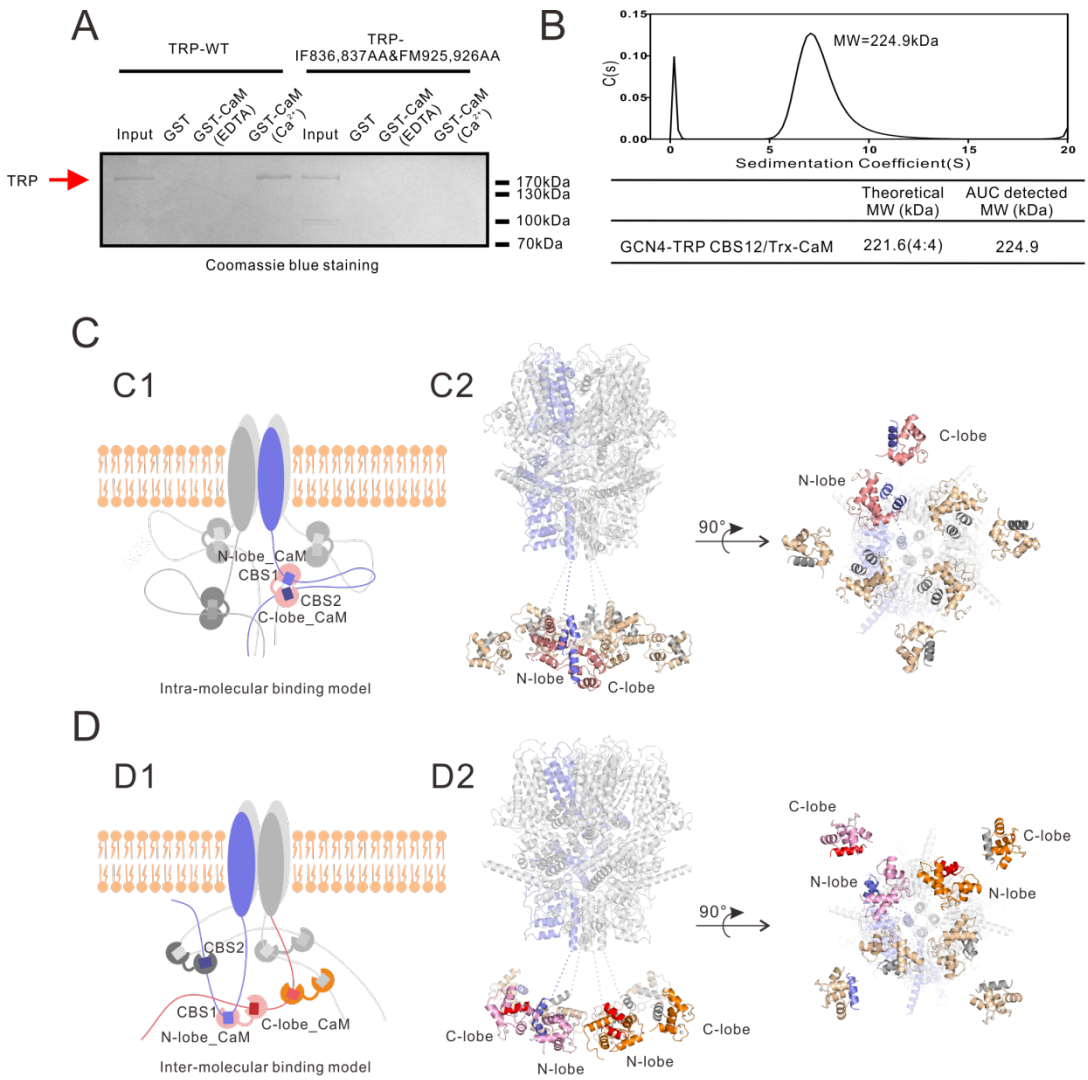

Figure 4: Ca^{2+}-dependent interaction between full-length TRP and CaM

(A) GST pull-down assay showing that endogenous TRP purified from fly heads interacted with CaM in a Ca^{2+}-dependent manner. GST-CaM had no detectable binding to TRP when Ca^{2+} in the assay buffer was chelated by EDTA. When IF836,837AA and FM925,926AA quadruple mutations were introduced to TRP (the quadruple mutations were introduced in a *trp* genomic rescue in a $trpl^{MB10553}$;$trp^{MB03672}$double null mutant background), the interaction between TRP and Ca^{2+}-CaM was totally abolished.

(B) Analytical ultracentrifugation sedimentation velocity assay showing the formation of a 4:4 complex between GCN4-CBS12 (TRP CBS12 fused to the C-terminal tail of a GCN4 coiled-coil tetramer) and Ca^{2+}-CaM.

(C&D) Schematic and ribbon diagrams showing that the two lobes of Ca^{2+}-CaM bind to CBS1 and CBS2 from the same molecule of the TRP tail (i.e. the intra-molecular binding model; C); or the two lobes of Ca^{2+}-CaM bind to CBS1

and CBS2 from two different subunits the TRP tails (i.e. the inter-molecular binding model; D). The models were generated by docking the TRP CBS1/N-lobe_CaM complex and TRP CBS2/C-lobe_CaM complex crystal structures on to the cryo-EM structure of TRPC4, PDB:5Z96.

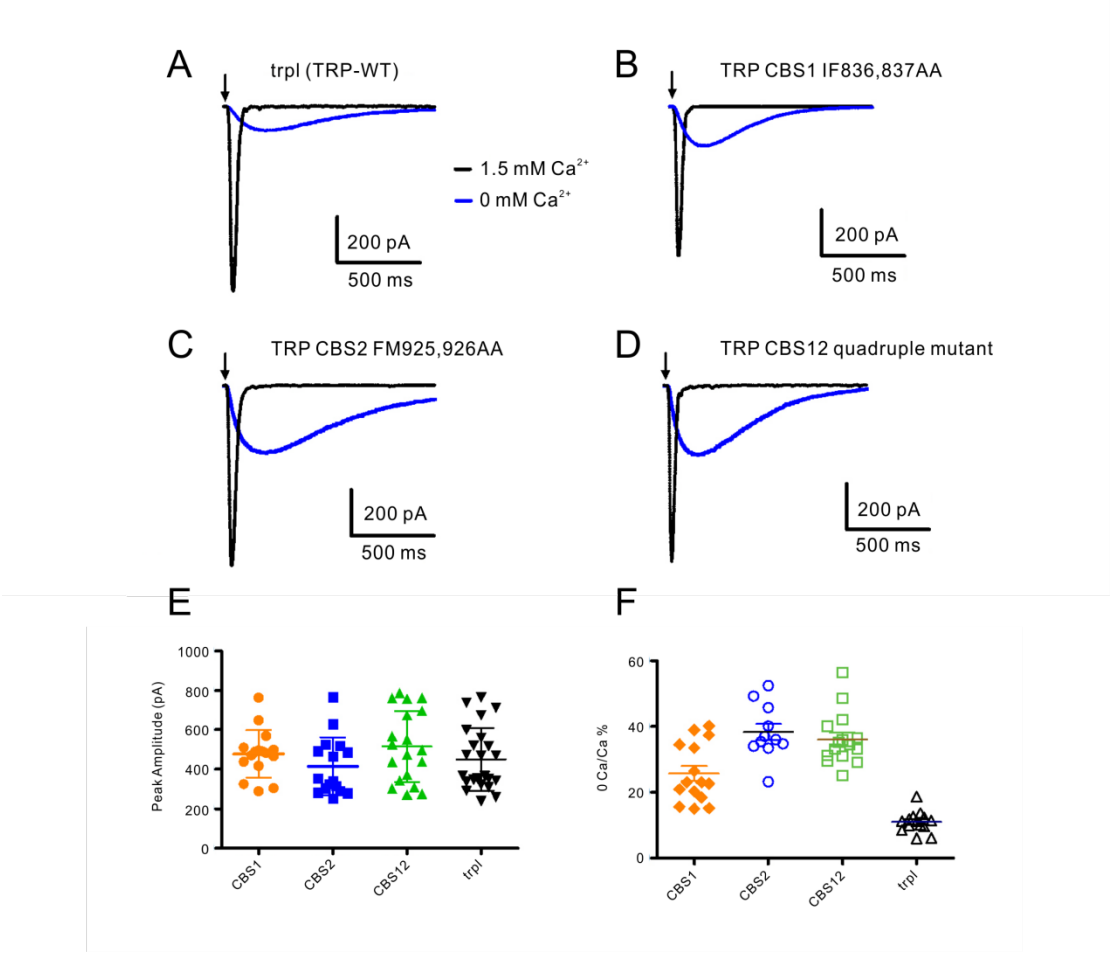

Figure 5: Disruptions of CaM binding to CBS1, CBS2 or CBS12 do not directly affect Ca^{2+}-mediated feedback on TRP channel activity

(A) Example responses to 1 ms flashes (arrows) containing ~150 effective photons in whole-cell patch-clamped TRP wild-type photoreceptors (in the *trpl* background) in the presence and absence of bath Ca^{2+}.

(B-D) Example responses to 1 ms flashes (arrows) (~150 effective photons) in photoreceptors from TRP CBS1 (B), CBS2 (C) and CBS1+2 mutants (in the $trpl^{MB10553};trp^{MB03672}$ background), in the presence and absence of bath Ca^{2+}.

(E) Quantification of peak response amplitude of photoreceptors expressing either TRP-WT (*trpl*) or Ca^{2+}-CaM binding mutants of TRP, in the presence of physiological Ca^{2+} (1.5 mM). Individual values and means ± SD are shown for WT (n=23 cells) and mutants (n=16-19). The four groups were not significantly different (p=0.26; one-way ANOVA)

(F) Percentage ratios of peak response amplitudes in 0 Ca^{2+} over physiological Ca^{2+} in the TRP-WT and mutants. Individual values and means ± SD are shown for WT

(n=14 cells) and mutants (n=11-15). The four groups were significantly different ($p<0.0001$; one-way ANOVA). In particular, all three mutants had larger ratios (i.e. larger relative 0 Ca^{2+} responses) compared to WT ($p<0.0001$ for each pair; Tukey's post test). Moreover, CBS2 and CBS1+2 both had significantly larger ratios compared to CBS1 ($p<0.001$ and $p<0.01$; Tukey's test).

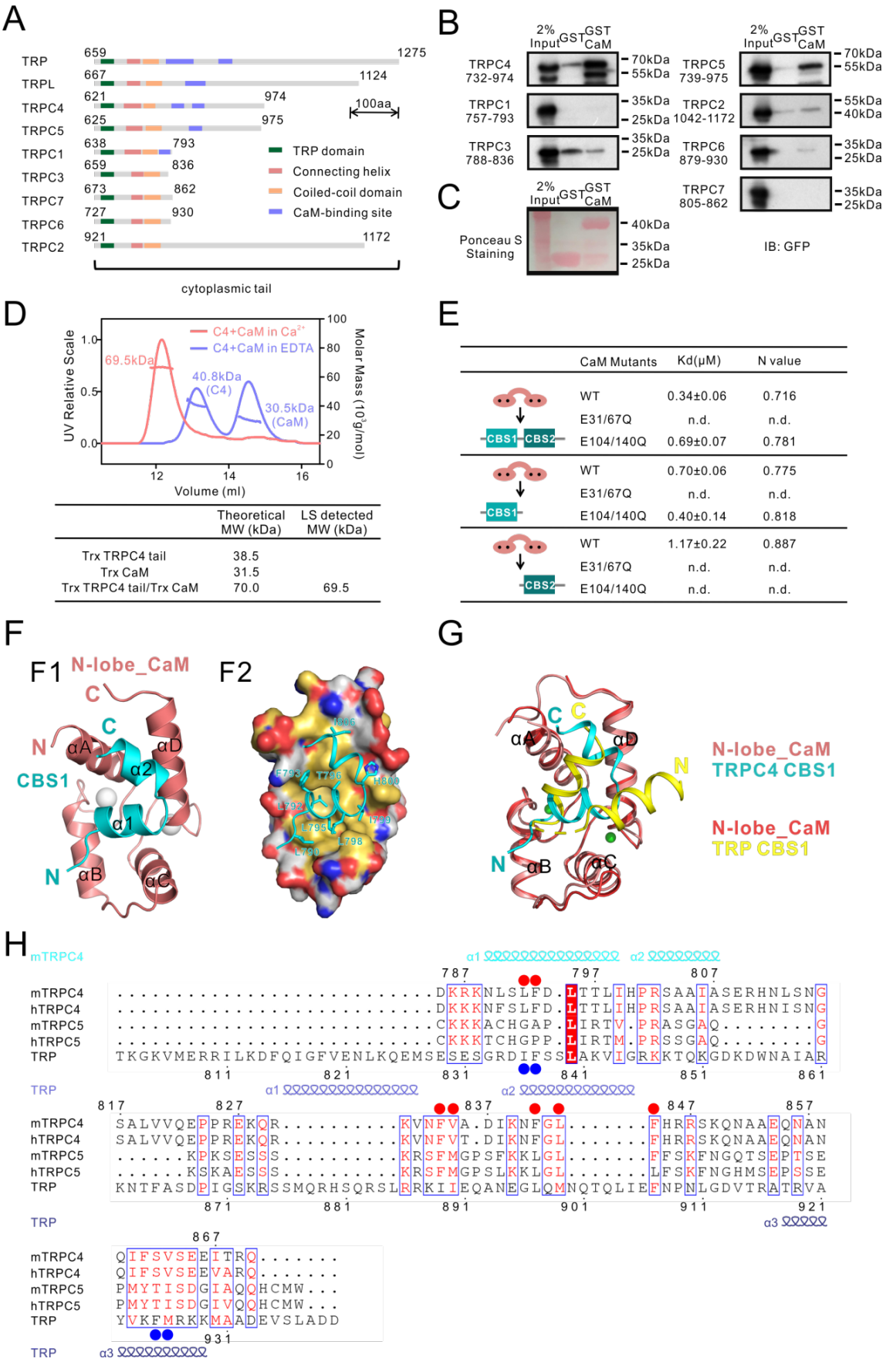
A
TRP
TRPL
TRPC4
TRPC5
TRPC1
TRPC3
TRPC7
TRPC6
TRPC2
659
1275
667
1124
621
974
625
975
638
793
659
836
673
862
727
930
921
1172
100aa
TRP domain
Connecting helix
Coiled-coil domain
CaM-binding site
cytoplasmic tail
B
2% Input
GST
GST CaM
TRPC4 732-974
TRPC1 757-793
TRPC3 788-836
TRPC5 739-975
TRPC2 1042-1172
TRPC6 879-930
TRPC7 805-862
70kDa
55kDa
35kDa
25kDa
40kDa
C
Ponceau S Staining
IB: GFP
D
C4+CaM in Ca2+
C4+CaM in EDTA
69.5kDa
40.8kDa (C4)
30.5kDa (CaM)
UV Relative Scale
Molar Mass (10³g/mol)
Volume (ml)
Theoretical MW (kDa)
LS detected MW (kDa)
Trx TRPC4 tail 38.5
Trx CaM 31.5
Trx TRPC4 tail/Trx CaM 70.0 69.5
E
CaM Mutants
Kd(μM)
N value
WT 0.34±0.06 0.716
E31/67Q n.d. n.d.
E104/140Q 0.69±0.07 0.781
WT 0.70±0.06 0.775
E31/67Q n.d. n.d.
E104/140Q 0.40±0.14 0.818
WT 1.17±0.22 0.887
E31/67Q n.d. n.d.
E104/140Q n.d. n.d.
CBS1
CBS2
F
F1 N-lobe_CaM
αA
αD
α2
α1
αB
αC
F2
G
N-lobe_CaM TRPC4 CBS1
N-lobe_CaM TRP CBS1
H
mTRPC4
hTRPC4
mTRPC5
hTRPC5
TRP

Figure 6: TRPC4 binds to Ca^{2+}-CaM following a similar mode as TRP does

(A) Schematic diagram showing the domain organizations of the C-terminal tails of *Drosophila* TRP, TRPL and the mouse TRPC subfamily members 1-7.

(B) GST pull down assay showing that Ca^{2+}-CaM only binds to the tails of TRPC4 and TRPC5.

(C) Ponceau S staining of GST and GST-CaM used in the pull-down assay in panel B.

(D) Analytical gel filtration coupled with static light scattering showing that TRPC4 forms a 1:1 molar ratio complex with CaM in a Ca^{2+}-dependent manner.

(E) Table summarizing the binding affinities of CaM to TRPC4 CBS12 (758-974), CBS1 (758-817), and CBS2 (818-974). The table also shows that the impact of Ca^{2+} binding deficient mutants of CaM in binding to CBS1, CBS2, and CBS12.

(F) Crystal structure of the TRPC4 CBS1 in complex with the N-lobe_CaM shown in the ribbon (F1) and surface combined with ribbon (F2) models with the same coloring scheme as in Figure 3B.

(G) Alignment of the TRP CBS1/N-lobe_CaM and the TRPC4 CBS1/N-lobe_CaM complexes showing the formation of the "helix-turn-helix" conformation of CBS1 from TRP (yellow) and from TRPC4 (cyan) upon binding to N-lobe of Ca^{2+}-CaM. The N-lobe_CaM structures were superimposed to each other in this alignment.

(H) Sequence alignment of CBS12 regions of TRP, TRPC4 and TRPC5 with the same coloring scheme as that in Figure 2A. The residues from TRPC4 CBS1 and CBS2 that are critical for CaM binding are indicated by red dots. The residues critical for CaM binding in TRP CBS1/2 are indicated by blue dots.

Supplemental Figures

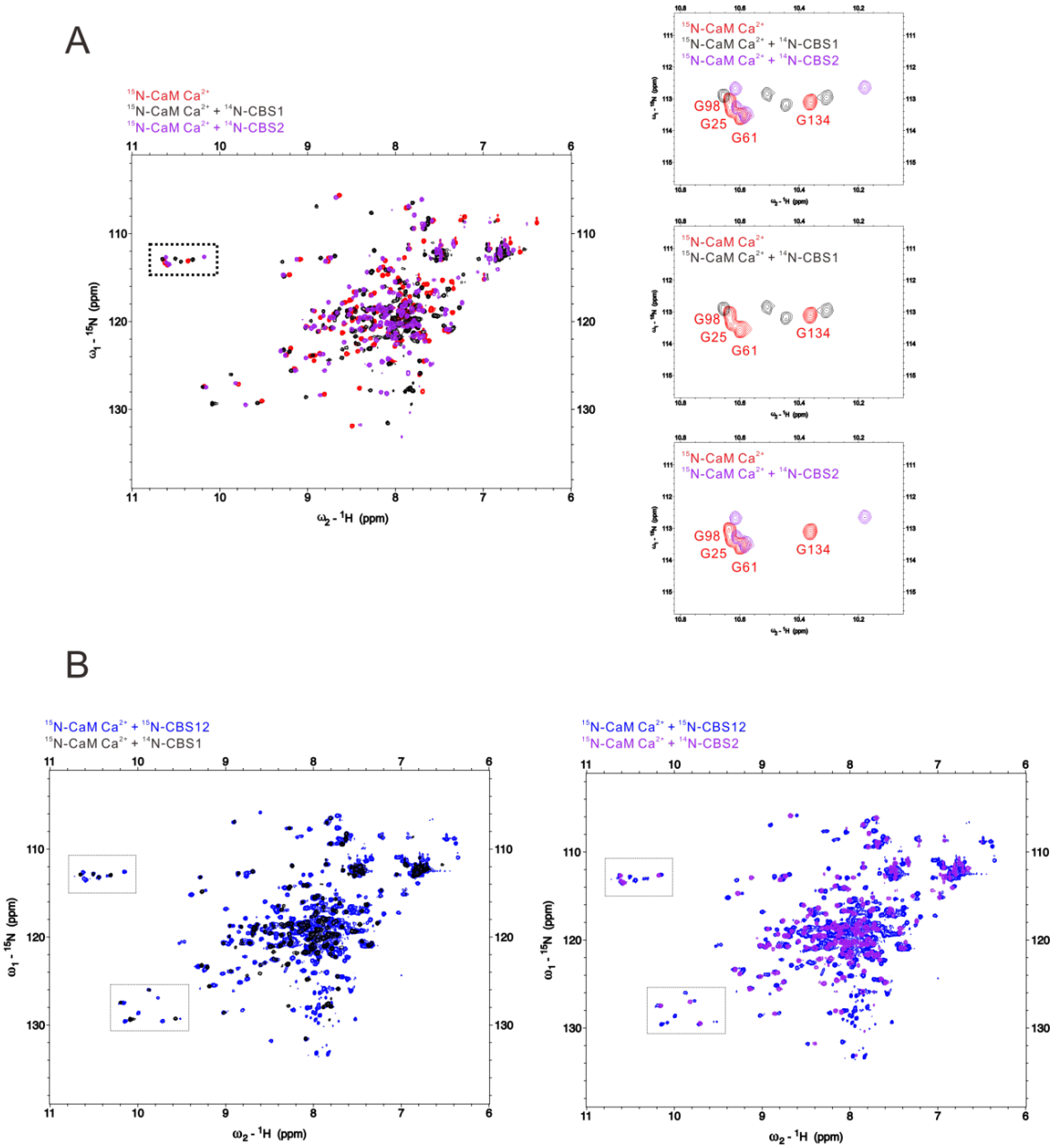

Figure S1: Overlay of the $^{1}H,^{15}N$-HSQC Spectra of ^{15}N-Ca^{2+}-CaM with different CaM binding sites of TRP

(A) Overlay of the $^{1}H,^{15}N$-HSQC spectra of ^{15}N-Ca^{2+}-CaM alone (red) and with those of ^{15}N-Ca^{2+}-CaM in complex with ^{14}N-TRP CBS1 (black) and CBS2 (purple), respectively. The region shown in the dashed box are the residues corresponding to the conserved Gly residue in each EF-hand of Ca^{2+}-bound CaM and is enlarged at the right for detailed comparison.

(B) Overlay of the $^{1}H,^{15}N$-HSQC spectrum of ^{15}N-Ca^{2+}-CaM in complex with

^{15}N-CBS12 (blue) with those of ^{15}N-Ca^{2+}-CaM in complex with ^{14}N-TRP CBS1 (black, left panel) and CBS2 (purple, right panel), respectively.

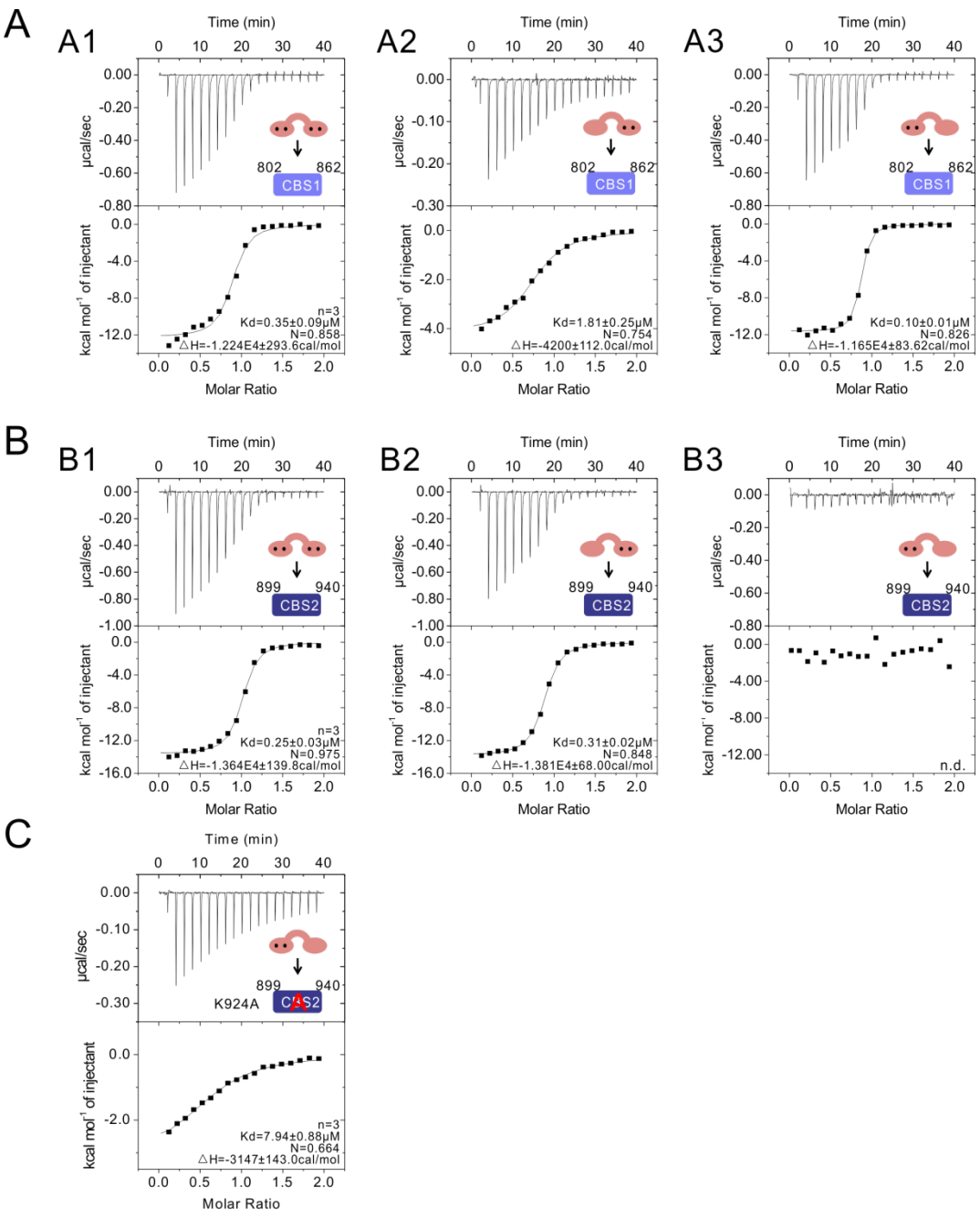

Figure S2: ITC-based measurements of the binding affinities of CaM mutants to TRP CBS1 and CBS2

(A) ITC-based measurements of the bindings of TRP CBS1 to CaM and its mutants: CaM WT (A1), CaM_E31/67Q (A2), CaM_E104/140Q (A3).

(B) ITC-based measurements of the binding of TRP CBS2 to CaM and its mutants: CaM WT (B1), CaM_E31/67Q (B2), CaM_E104/140Q (B3).

(C) ITC-based measurement of the binding of TRP CBS2 K924A to CaM E104/140Q.

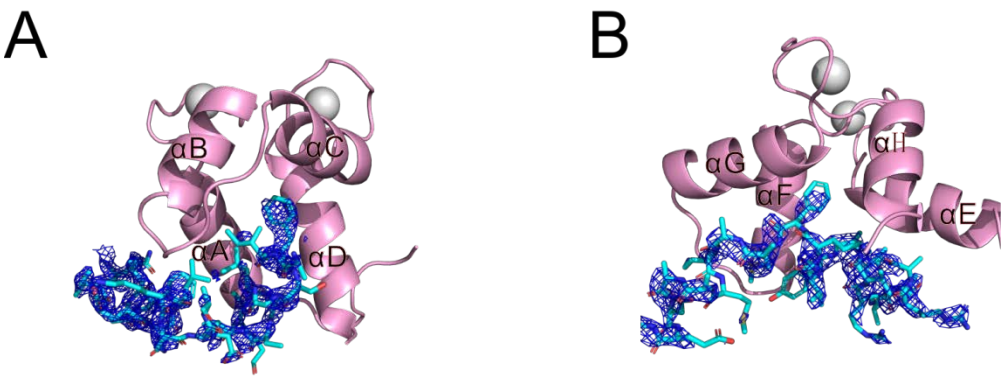

Figure S3: Omit map of the TRP CBS1/N-lobe_CaM complex and the TRP CBS2/C-lobe_CaM complex

(A) Omit map of the α1 and α2 helices of CBS1 in complex with CaM N-lobe. The Fo-Fc density map was generated by deleting α1 and α2 and contoured at 2.5σ.

(B) Omit map of CBS2 α3 bound to CaM C-lobe. The Fo-Fc density map was generated by deleting α3 and contoured at 2.5σ.

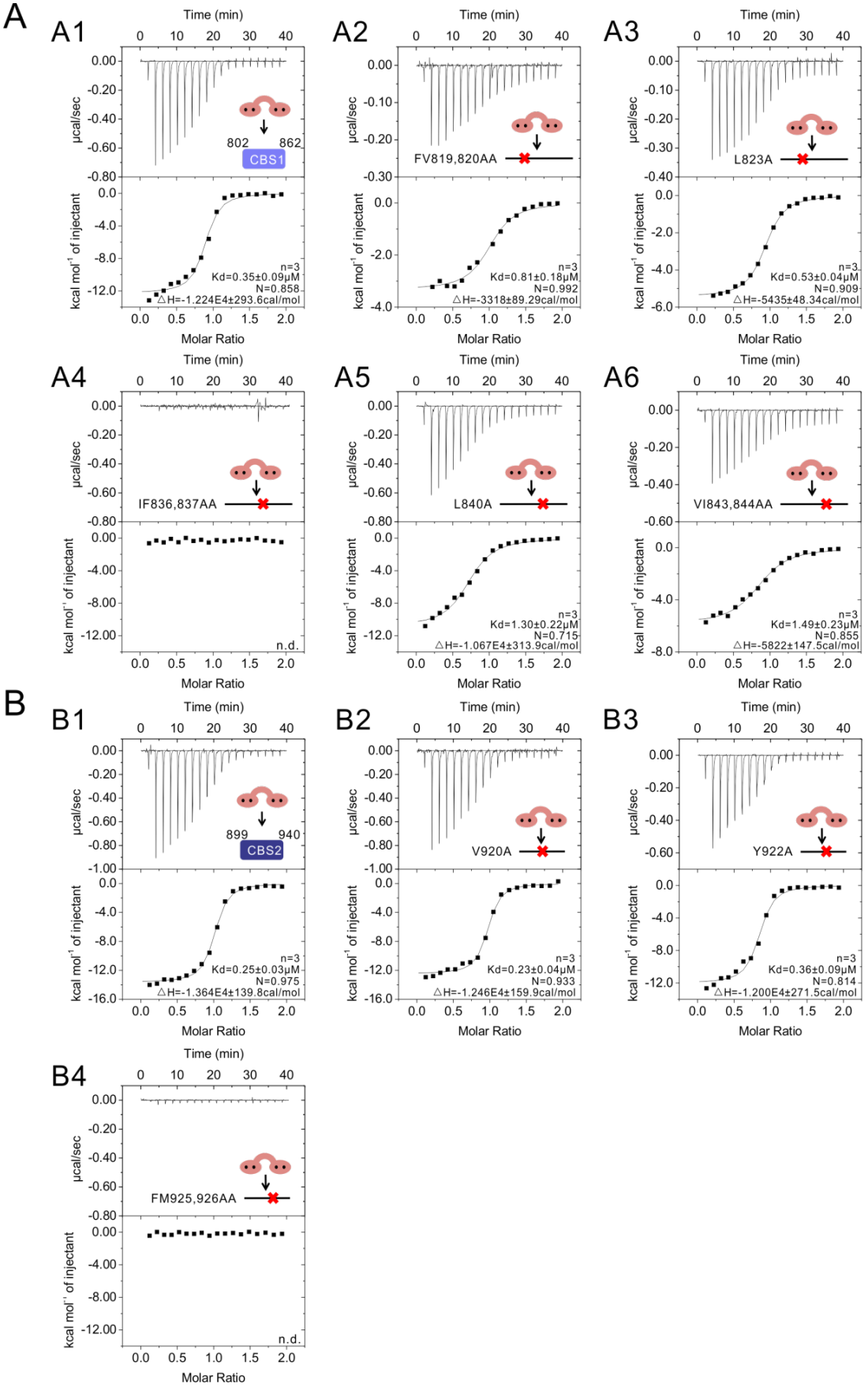
A
A1
Time (min)
µcal/sec
kcal mol⁻¹ of injectant
802
862
CBS1
n=3
Kd=0.35±0.09µM
N=0.858
△H=-1.224E4±293.6cal/mol
Molar Ratio
A2
FV819,820AA
n=3
Kd=0.81±0.18µM
N=0.992
△H=-3318±89.29cal/mol
A3
L823A
n=3
Kd=0.53±0.04µM
N=0.909
△H=-5435±48.34cal/mol
A4
IF836,837AA
n.d.
A5
L840A
n=3
Kd=1.30±0.22µM
N=0.715
△H=-1.067E4±313.9cal/mol
A6
VI843,844AA
n=3
Kd=1.49±0.23µM
N=0.855
△H=-5822±147.5cal/mol
B
B1
899
940
CBS2
n=3
Kd=0.25±0.03µM
N=0.975
△H=-1.364E4±139.8cal/mol
B2
V920A
n=3
Kd=0.23±0.04µM
N=0.933
△H=-1.246E4±159.9cal/mol
B3
Y922A
n=3
Kd=0.36±0.09µM
N=0.814
△H=-1.200E4±271.5cal/mol
B4
FM925,926AA
n.d.

Figure S4: ITC-based measurements of the binding affinities of Ca^{2+}-CaM to TRP CBS1 and CBS2 mutants

(A) ITC-based measurements of the bindings of Ca^{2+}-CaM to different TRP CBS1 mutants: CBS1 WT (A1), CBS1 FV819,820AA (A2), CBS1 L823A (A3), CBS1 IF836,837AA (A4), CBS1 L840A (A5), and CBS1 VI843,844AA (A6).

(B) ITC-based measurements of the bindings of Ca^{2+}-CaM to TRP CBS2 mutants: CBS2 WT (B1), CBS2 V920A (B2), CBS2 Y922A (B3), and CBS2 FM925,926AA (B4).

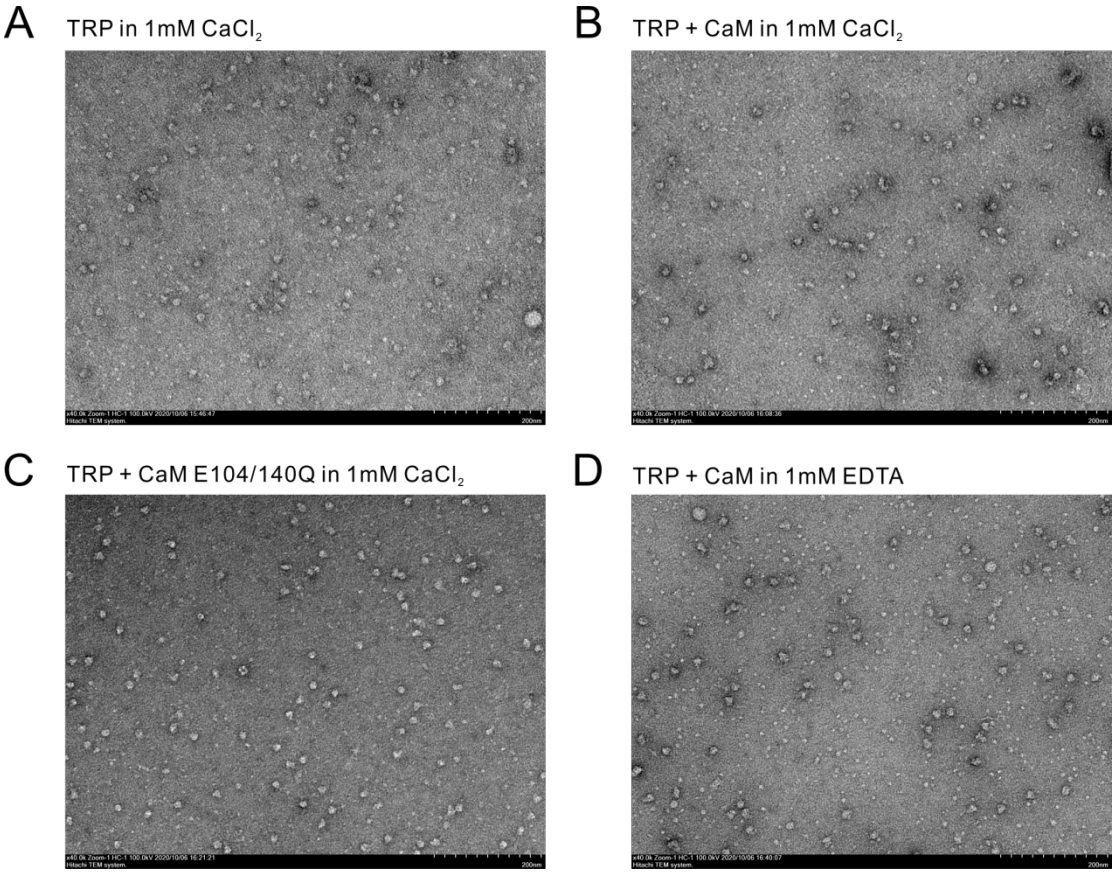

Figure S5. Negative staining TEM images of purified endogenous TRP with or without addition of CaM.

(A) TRP alone in 1mM $CaCl_2$. (B) TRP:CaM = 1:1 in 1mM $CaCl_2$. (C) TRP:CaM(E104/140Q) = 1:1 in 1mM $CaCl_2$. (D) TRP:CaM = 1:1 in 1mM EDTA.

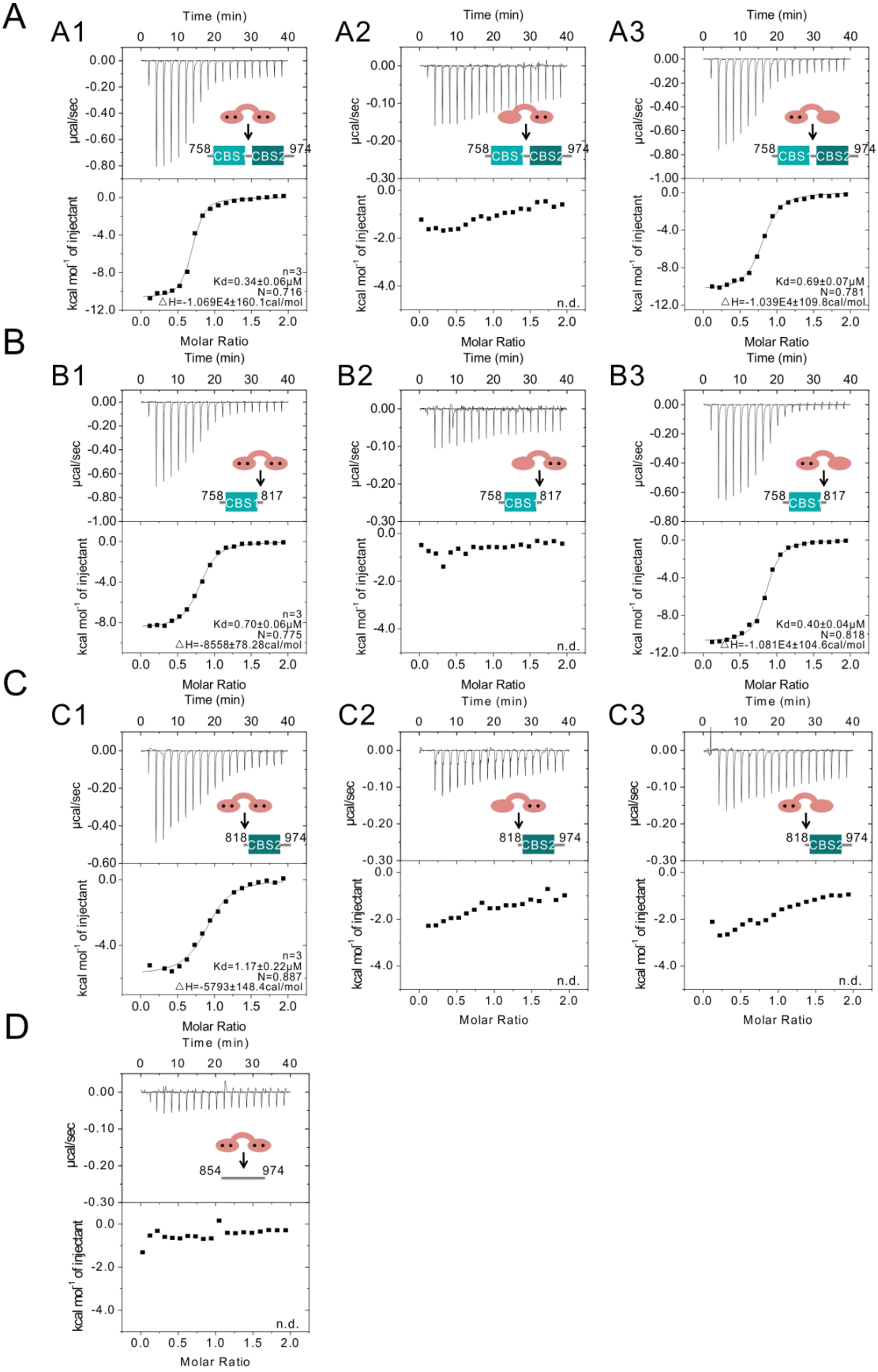
A
A1
Time (min)
µcal/sec
kcal mol-1 of injectant
758
CBS1
CBS2
974
n=3
Kd=0.34±0.06µM
N=0.716
△H=-1.069E4±160.1cal/mol
Molar Ratio
A2
n.d.
A3
Kd=0.69±0.07µM
N=0.781
△H=-1.039E4±109.8cal/mol
B
B1
817
Kd=0.70±0.06µM
N=0.775
△H=-8558±78.28cal/mol
B2
B3
Kd=0.40±0.04µM
N=0.818
△H=-1.081E4±104.6cal/mol
C
C1
818
Kd=1.17±0.22µM
N=0.887
△H=-5793±148.4cal/mol
C2
C3
D
854

Figure S6: ITC-based measurements of the binding affinities of CaM mutants to TRPC4 fragments

(A) ITC-based measurements of the binding affinities of CaM (A1) and its Ca^{2+} binding deficient mutants E31/67Q (A2) and E104/140Q (A3) to TRPC4 CBS12.

(B) ITC-based measurements of the binding affinities of CaM (B1) and its Ca^{2+} binding deficient mutants E31/67Q (B2) and E104/140Q (B3) to TRPC4 CBS1 (758-817).

(C) ITC-based measurements of the binding affinities of TRPC4 CBS2(817-974) to CaM (C1) and its Ca^{2+} binding deficient mutants: E31/67Q (C2) and E104/140Q (C3).

(D) ITC-based measurement of the binding affinity of CaM to the TRPC4 C-terminal fragment (854-974).

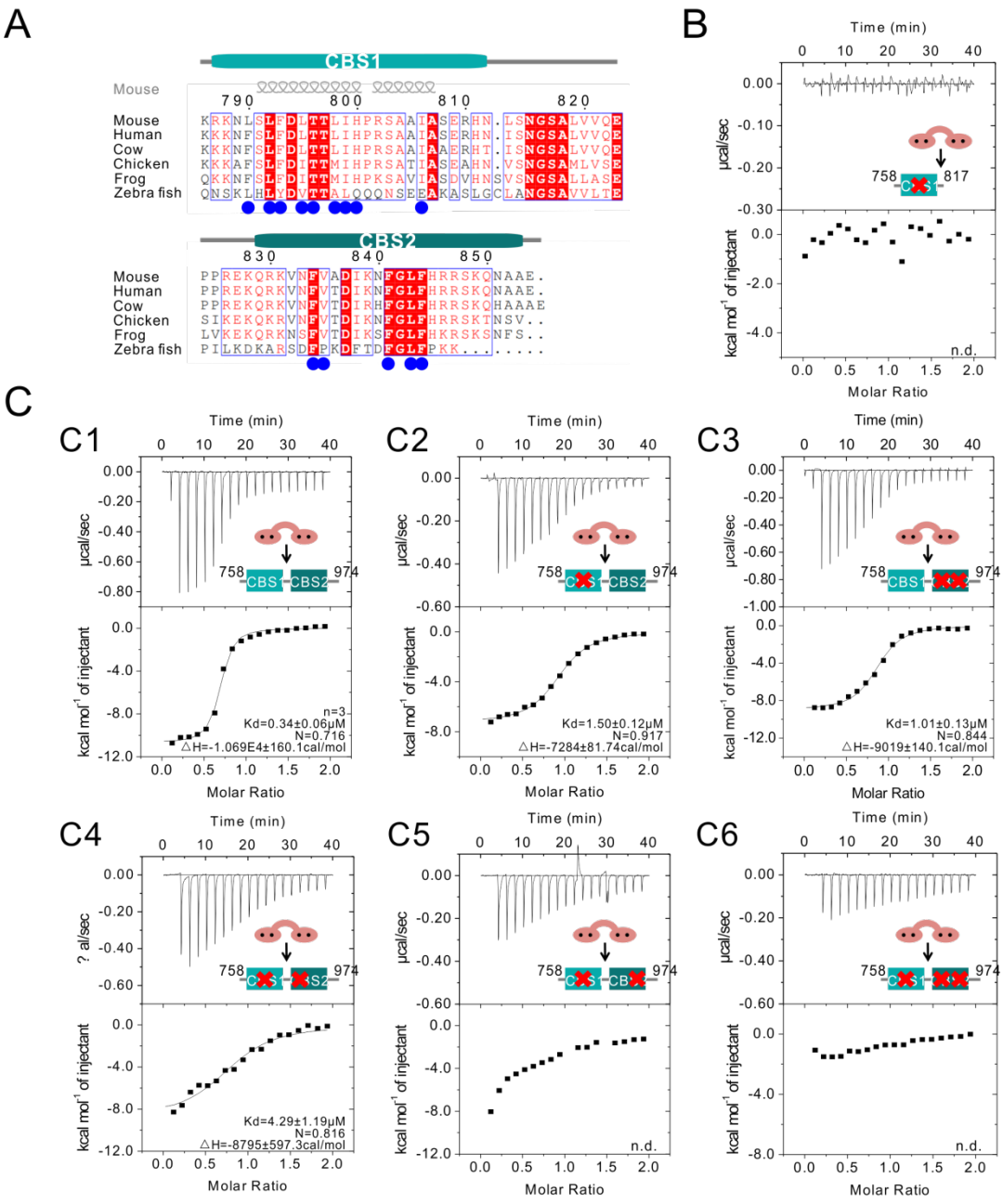

Figure S7: ITC-based measurements of the bindings of CaM to TRPC4 mutants

(A) Sequence alignment of CBS12 of TRPC4 from different species with the same coloring scheme as that in Figure 2A. The residues from TPRC4 CBS1 and CBS2 that are critical for CaM binding are indicated by blue dots.

(B) ITC-based measurement of the binding affinity of CaM to TRPC4 CBS1(758-817) LF792,793AA.

(C) ITC-based measurements of the binding affinities of CaM to TRPC4 (758-974) mutants: TRPC4 WT (C1), TRPC4 LF792,793AA (C2), TRPC4

FV834,835AA&FGLF841,842,843,844AGAA (C3), TRPC4 LFtoAA&FVtoAA (C4), TRPC4 LFtoAA&FGLFtoAGAA (C5), and TRPC4 LFtoAA&FVtoAA&FGLFtoAGAA (C6).

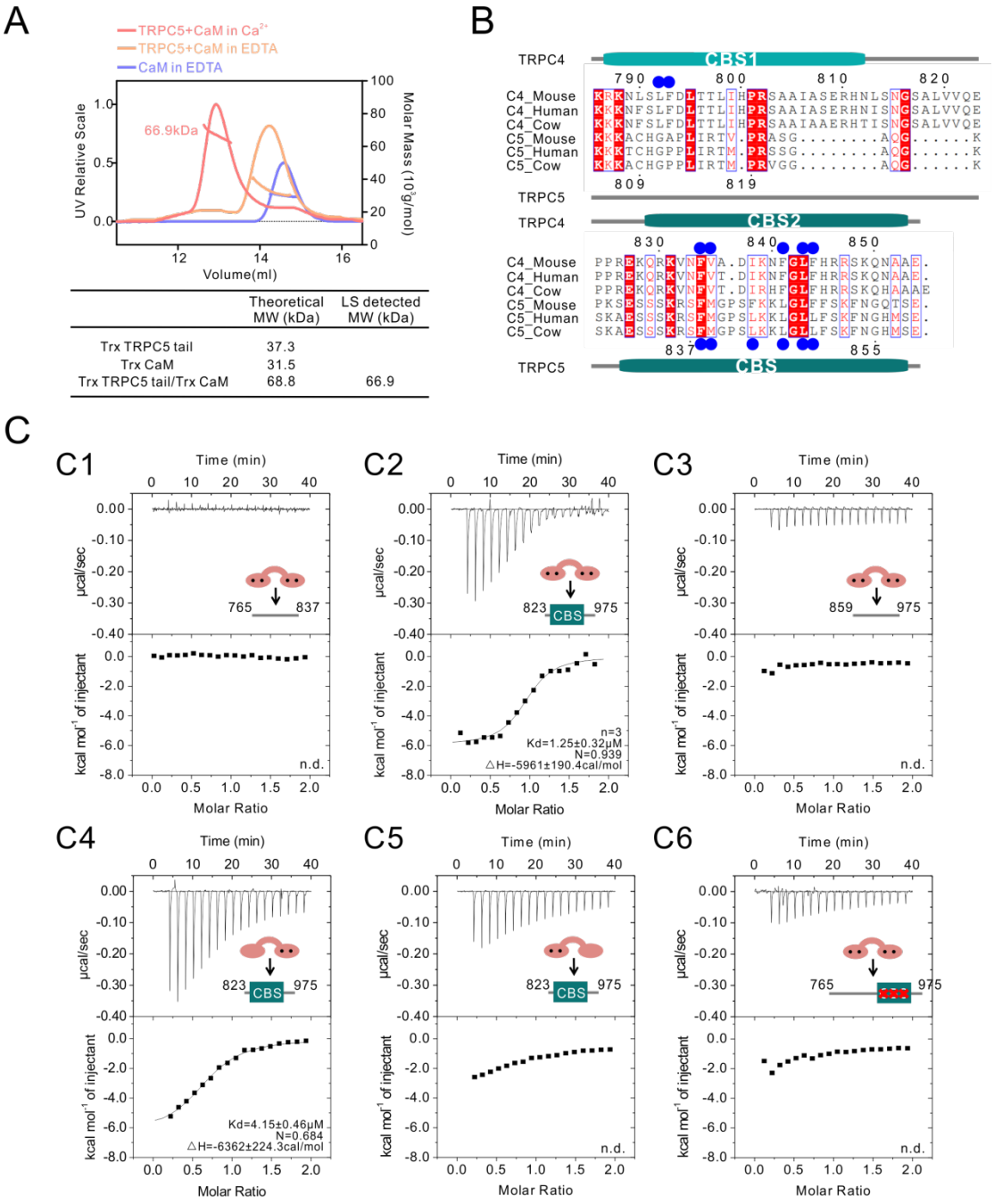

	Theoretical MW (kDa)	LS detected MW (kDa)
Trx TRPC5 tail	37.3	
Trx CaM	31.5	
Trx TRPC5 tail/Trx CaM	68.8	66.9

Figure S8: TRPC5 C-terminal tail interacts with CaM in a Ca^{2+}-dependent manner

(A) Analytical gel filtration coupled with static light scattering showing that TRPC5 tail forms a 1:1 complex with CaM in a Ca^{2+}-dependent manner.

(B) Sequence alignment between TRPC4 and TRPC5 corresponding to the CBS12 region of TRPC4. Note that the TRPC5 tail does not contain critical residues corresponding to CBS1 in TRPC4. The residues for critical for CaM interaction in TRPC4 and TRPC5 CBSs are indicated by blue dots.

(C) ITC-based measurements of the binding affinities of CaM and its mutants to different TRPC5 C-terminal fragments: CaM WT to TRPC5 (765-837, C1), CaM WT to TRPC5 CBS (822-975, C2), CaM WT to TRPC5 very C-terminal fragment(859-975, C3), CaM E31/67Q to TRPC5 CBS (822-975, C4), CaM E104/140Q to TRPC5 CBS (822-975, C4), and CaM WT to TRPC5 FM838,839AA&F843A&LGLF846,847,848,849AGAA (765-975, C6).